Article

Developmental Cell

Canonical Wnt5b Signaling Directs Outlying Nkx2.5+ Mesoderm into Pacemaker Cardiomyocytes

Graphical Abstract

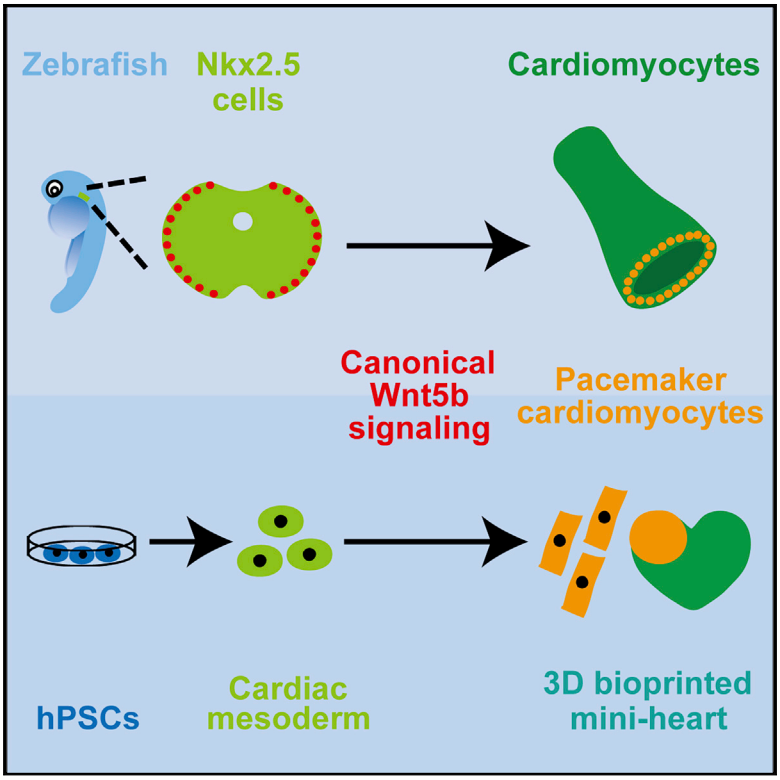

Highlights

- Pacemaker cardiomyocytes derive from a subset of Nkx2.5+ mesoderm
- Canonical Wnt5b signaling directs pacemaker cardiomyocyte differentiation *in vivo*
- Wnt5b signaling promotes hPSC-pacemaker cardiomyocyte differentiation *in vitro*
- hPSC-pacemaker cardiomyocytes can pace 3D bioprinted hPSC-cardiomyocytes

Authors

Jie Ren, Peidong Han, Xuanyi Ma, ..., Deborah Yelon, Shaochen Chen, Neil C. Chi

Correspondence

nchi@ucsd.edu

In Brief

Pacemaker cardiomyocytes are crucial for maintaining heart rate. Ren et al. show that these specialized cardiomyocytes originate from outlying Nkx2.5+ mesoderm that responds to canonical Wnt5b signaling in zebrafish. Applying these findings to human pluripotent stem cells (hPSCs) results in the generation of hPSC-pacemaker cardiomyocytes that can pace bioprinted hPSC-cardiomyocytes.

Ren et al., 2019, Developmental Cell *50*, 729–743
September 23, 2019 Published by Elsevier Inc.
https://doi.org/10.1016/j.devcel.2019.07.014

CellPress

Developmental Cell
Article

Canonical Wnt5b Signaling Directs Outlying Nkx2.5+ Mesoderm into Pacemaker Cardiomyocytes

Jie Ren,[1] Peidong Han,[1] Xuanyi Ma,[2] Elie N. Farah,[1] Joshua Bloomekatz,[1,3] Xin-Xin I. Zeng,[4] Ruilin Zhang,[1] Megan M. Swim,[1] Alec D. Witty,[1] Hannah G. Knight,[4] Rima Deshpande,[1] Weizhe Xu,[2] Deborah Yelon,[4] Shaochen Chen,[2,5,6] and Neil C. Chi[1,6,7,8,*]

[1]Department of Medicine, Division of Cardiology, University of California, San Diego, La Jolla, CA 92093, USA
[2]Department of Bioengineering, University of California, San Diego, La Jolla, CA 92093, USA
[3]Department of Biology, University of Mississippi, Oxford, MS 38677, USA
[4]Division of Biological Sciences, University of California, San Diego, La Jolla, CA 92093, USA
[5]Department of NanoEngineering, University of California, San Diego, La Jolla, CA 92093, USA
[6]Institute for Engineering in Medicine, University of California, San Diego, La Jolla, CA 92093, USA
[7]Institute of Genomic Medicine, University of California, San Diego, La Jolla, CA 92093, USA
[8]Lead Contact
*Correspondence: nchi@ucsd.edu
https://doi.org/10.1016/j.devcel.2019.07.014

SUMMARY

Pacemaker cardiomyocytes that create the sinoatrial node are essential for the initiation and maintenance of proper heart rhythm. However, illuminating developmental cues that direct their differentiation has remained particularly challenging due to the unclear cellular origins of these specialized cardiomyocytes. By discovering the origins of pacemaker cardiomyocytes, we reveal an evolutionarily conserved Wnt signaling mechanism that coordinates gene regulatory changes directing mesoderm cell fate decisions, which lead to the differentiation of pacemaker cardiomyocytes. We show that in zebrafish, pacemaker cardiomyocytes derive from a subset of Nkx2.5+ mesoderm that responds to canonical Wnt5b signaling to initiate the cardiac pacemaker program, including activation of pacemaker cell differentiation transcription factors Isl1 and Tbx18 and silencing of Nkx2.5. Moreover, applying these developmental findings to human pluripotent stem cells (hPSCs) notably results in the creation of hPSC-pacemaker cardiomyocytes, which successfully pace three-dimensional bioprinted hPSC-cardiomyocytes, thus providing potential strategies for biological cardiac pacemaker therapy.

INTRODUCTION

The heart consists of a multitude of diverse cardiomyocyte cell types, including atrial, ventricular, and pacemaker cells, which cooperate to ensure proper cardiac function and circulation throughout the body. Because loss or dysfunction of these cell types can lead to severe cardiac arrhythmias or heart failure, increasing efforts have been recently devoted toward understanding how these cardiomyocytes are created in order to develop potential human cardiac regenerative therapies (Laflamme and Murry, 2011). Such endeavors have illuminated not only the origins of many cardiomyocyte lineages (Cai et al., 2003; Stanley et al., 2002) but also key signaling cues and transcriptional regulators, which in turn have been employed to efficiently direct various non-cardiac sources including human pluripotent stem cells (hPSCs) and human fibroblasts into specific cardiomyocyte cell types (Cao et al., 2016; Lian et al., 2012; Wada et al., 2013).

Although a large portion of cardiomyocytes derives from two temporally and spatially distinct Nkx2.5+ progenitor populations (Stanley et al., 2002), namely the first and second heart fields (FHF, SHF), the developmental source of pacemaker cardiomyocytes (CMs) remains less certain despite the discovery of these specialized pacing cardiomyocytes more than 100 years ago (Keith and Flack, 1907; Trautwein and Uchizono, 1963). Illuminating their developmental origins has been particularly challenging due to their atypical cardiomyocyte characteristics including the lack of Nkx2.5 expression, which distinguishes them from most other cardiomyocytes (Wiese et al., 2009). As a result, recent studies suggest that pacemaker CMs may originate from an additional Nkx2.5-negative heart field that is developmentally and molecularly distinct from the aforementioned well-established Nkx2.5+ heart fields (Bressan et al., 2013). However, others propose that they may arise from the outlying regions within these Nkx2.5+ heart fields where the transcription factor Shox2 may reduce Nkx2.5 expression during pacemaker CM differentiation (Lescroart et al., 2012; Liang et al., 2013; Mommersteeg et al., 2010). In line with this notion, Shox2 is specifically expressed in the sinoatrial node (SAN) region and has been shown to be required for pacemaker development through inhibiting Nkx2.5 expression (Blaschke et al., 2007; Espinoza-Lewis et al., 2009). Finally, given the heterogeneity of cardiomyocytes within the SAN (Liang et al., 2015; Sun et al., 2007), pacemaker CMs alternatively may derive from multiple progenitor sources.

Along with Shox2, the transcription factors Isl1, Tbx3, and Tbx18 are coordinately expressed to control cardiomyocyte-pacemaker differentiation through not only activating genes specific for pacemaker cell differentiation and function but also inhibiting genes involved in the differentiation and function of atrial or ventricular chamber cardiomyocytes (van Weerd and

Christoffels, 2016). Although Isl1 regulates the specification of SHF progenitors and is downregulated during the differentiation of these cardiac progenitors into cardiomyocytes (Bu et al., 2009; Cai et al., 2003), Isl1 is also expressed in differentiated pacemaker CMs in order to activate genes required for pacemaker development and function including *Shox2*, *Tbx3*, and *Hcn4* (Liang et al., 2015; Sun et al., 2007; Tessadori et al., 2012; Vedantham et al., 2015). On the other hand, Shox2, Tbx3, and Tbx18 are expressed in pacemaker CMs to reinforce the differentiation of these specialized cardiomyocytes through preventing the activation of the cardiac chamber program (Blaschke et al., 2007; Christoffels et al., 2006; Espinoza-Lewis et al., 2009; Kapoor et al., 2013; Mommersteeg et al., 2007; Wiese et al., 2009); however, Tbx3 may also serve to activate genes required for pacemaker CM function as well (Bakker et al., 2012; Hoogaars et al., 2007). Because these factors coordinate a gene regulatory network that ensures proper pacemaker CM formation and function, the combined expression of these factors along with the cardiac conduction ion channel *Hcn4* (Stieber et al., 2003) has been utilized in recent pacemaker studies to define pacemaker CMs (Birket et al., 2015; Liang et al., 2015; Mommersteeg et al., 2007; Protze et al., 2017; Wiese et al., 2009).

Several signaling pathways have recently been implicated in pacemaker CM development, including bone morphogenetic protein (BMP) and Wnt signaling (Birket et al., 2015; Bressan et al., 2013; Protze et al., 2017). In particular, canonical Wnt signaling has been shown in chick studies to specify mesodermal cells outside the FHF and SHFs to the pacemaker lineage during early gastrulation (Bressan et al., 2013), despite its other roles during cardiac development including the induction of cardiac mesoderm formation at pre-gastrulation (Barrow et al., 2007; Liu et al., 1999; Ueno et al., 2007) and the specification of SHF progenitors and the inhibition of their differentiation into cardiomyocytes (Ai et al., 2007; Cohen et al., 2007; Kwon et al., 2007, 2009; Lin et al., 2007; Qyang et al., 2007). Furthermore, previous mouse studies have revealed that canonical Wnt signaling is activated in the SAN during heart development and conditional deletion of β-catenin leads to decreased expression of several cardiac genes including *Isl1*, *Pitx2*, and *Tbx3* (Lin et al., 2007), which are involved in pacemaker CM development (Bakker et al., 2012; Hoogaars et al., 2007; Liang et al., 2015; Mommersteeg et al., 2007; Tessadori et al., 2012; van Weerd and Christoffels, 2016; Vedantham et al., 2015; Wang et al., 2014; Wiese et al., 2009). Although these findings suggest that canonical Wnt signaling may regulate pacemaker CM differentiation possibly through Isl1, the specific Wnt ligands, the precise mesodermal cells that create these pacemaker CM lineages, and the underlying mechanisms by which canonical Wnt signaling along with other signals direct pacemaker CM formation remain to be elucidated.

To clarify the developmental source of pacemaker CMs, illuminate the coordinated signaling pathways directing their differentiation, and understand how these signaling pathways may activate the pacemaker CM program, we take advantage of the unique strengths of the zebrafish embryo to precisely fate map cardiac mesoderm *in vivo* using photoconversion lineage tracing strategies, and furthermore identify the specific Wnt ligand responsible for directing the differentiation of cardiac progenitor cells to pacemaker CMs. Specifically, we reveal that pacemaker CMs derive from outlying Nkx2.5+ progenitors that are located at the most lateral regions of the cardiac mesoderm. In response to Wnt5b, these Nkx2.5+ progenitors initiate canonical Wnt signaling to induce pacemaker CM differentiation through not only directly activating pacemaker differentiation transcription factors Isl1 and Tbx18 but also silencing Nkx2.5. Utilizing a combination of inducible genetic and chemical loss- and gain-of-function studies, we further discover that perturbing this canonical Wnt signaling reciprocally alters the allocation of Nkx2.5+ progenitors to prospective Nkx2.5− pacemaker or Nkx2.5+ atrial cardiomyocyte lineages, thus uncovering an important role for Wnt5b in partitioning the outlying regions of Nkx2.5+ mesoderm into a distinct cardiac progenitor pool for the pacemaker CM lineage. Moreover, by applying these developmental findings to hPSCs, we generate hPSC-derived pacemaker-like cardiomyocytes that can pace 3D bioprinted hPSC-cardiomyocytes. Overall, our findings reveal a new role for canonical Wnt signaling during cardiac development, which choreographs gene regulatory changes directing pacemaker CM differentiation.

RESULTS

Pacemaker CMs Originate from Peripherally Located Nkx2.5+ Progenitors

To begin to address the developmental source of pacemaker CMs, we used the zebrafish embryo to explore whether pacemaker CMs, which typically do not express Nkx2.5 (Wiese et al., 2009), derive from Nkx2.5+ cardiac progenitors prior to their differentiation. To this end, we tracked the fate of specific Nkx2.5+ cells during heart development through spatiotemporally marking distinct Nkx2.5+ cells using the *TgBAC(-36nkx2.5:Kaede)* [or *Tg(nkx2.5:Kaede)*] line, which expresses the stable photoconvertible Kaede protein in Nkx2.5+ cells. Photoconversion of all *nkx2.5:*Kaede+ cells from green to red at the 14 somite stage (ss), the earliest time point in which *nkx2.5*:Kaede is observable in the anterior lateral plate mesoderm (ALPM) (Guner-Ataman et al., 2013), reveals that Nkx2.5+ cardiac precursors produce not only atrial and ventricular cardiomyocytes but also inflow tract pacemaker CMs expressing Isl1, a key transcriptional regulator of pacemaker CM formation (Liang et al., 2015; Tessadori et al., 2012; Vedantham et al., 2015) by 24 h post-fertilization (hpf) (Figures 1A–1E’’’). In addition to not only expressing Isl1 and *myl7:*Cerulean, a marker for differentiated cardiomyocytes (Yelon et al., 1999), these photoconverted *nkx2.5:*Kaede+ inflow tract pacemaker CMs no longer exhibit the early cardiac developmental marker Nkx2.5, a distinctive feature of pacemaker CMs (Figures 1D–1E’’’, yellow arrowheads). To refine the location of these cardiac pacemaker precursors, we next spatially restricted our photoconversion to specific regions of the Nkx2.5+ ALPM domain. Consistent with previous cardiac mesodermal fate-mapping studies (Fukui et al., 2018; Mommersteeg et al., 2010), photoconversion at the most lateral edge of this Nkx2.5+ domain marks *nkx2.5:*Kaede+ cardiac progenitors, which become pacemaker CMs as well as atrial cardiomyocytes near the inflow region by 24 hpf (Figures 1F–1J’’’, 1P, and 1Q). On the other hand, photoconversion along the medial edge labels *nkx2.5:*Kaede+ cardiac progenitors that primarily develop into ventricular cardiomyocytes that express *myl7:*Cerulean and Nkx2.5, but not Isl1 (Figures 1K–1O’’’, 1P, and 1Q).

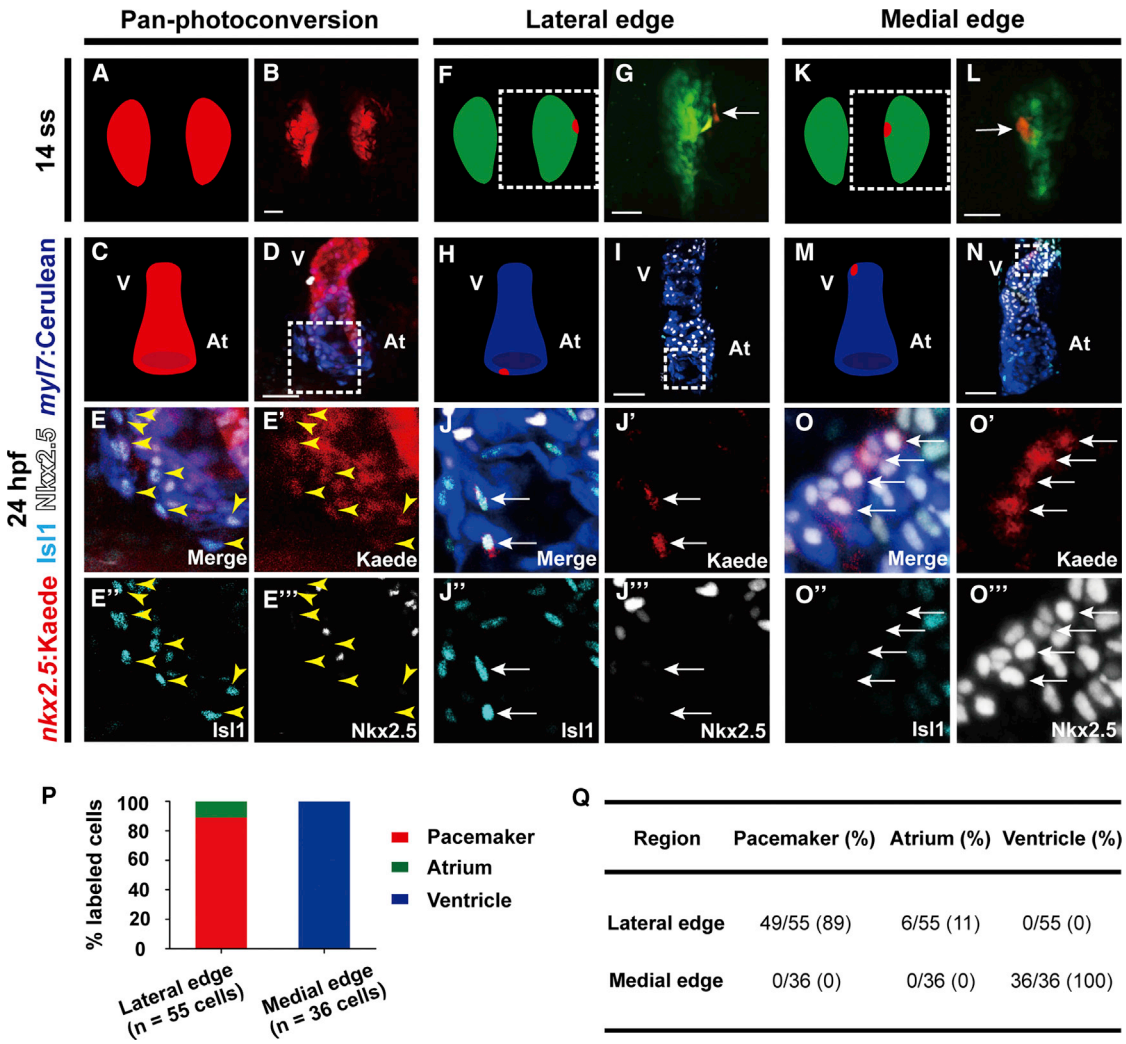

Figure 1. Pacemaker Cells Originate from the Most Lateral Edge of the *nkx2.5*+ Progenitor Fields Residing within the ALPM

Confocal imaging of *Tg(nkx2.5:Kaede; myl7:Cerulean)* embryos shows the location of *nkx2.5:*Kaede cells immediately after photoconversion at (B, G, and L) 14 ss as well as respectively later at (D, E, I, J, N, and O) 8 h post-photoconversion at 24 hpf. Immunostaining detects Isl1 and Nkx2.5-expressing cells. (A, C, F, H, K, and M) Schematics illustrate the position of photoconverted (red) and non-photoconverted (green) *nkx2.5:*Kaede cells as well as *myl7*:Cerulean cardiomyocytes (blue) for (B), (D), (G), (I), (L), and (N) images, respectively. (A–E''') Pan-photoconversion of *Tg(nkx2.5:Kaede; myl7:Cerulean)* embryos at 14 ss results in photoconverted *nkx2.5:*Kaede+ Isl1+ *myl7:*Cerulean+ pacemaker cardiomyocytes at 24 hpf (n = 201/212 Isl1+ *myl7:*Cerulean+ pacemaker cardiomyocytes from 8 embryos). (F–O''') Localized photoconversion of *nkx2.5:*Kaede at the (F–J''') lateral or (K–O''') medial edge at 14 ss reveals that the lateral edge of *nkx2.5*+ cardiac mesoderm but not the medial edge contributes to pacemaker cardiomyocytes at 24 hpf. (E–E''', J–J''', O–O''', G, and L) Insets are magnifications of boxed areas in (D), (I), (N), (F), and (K), respectively. Images (E'–E'''), (J'–J'''), and (O'–O''') are single channels from (E), (J), and (O) merged images, respectively. Yellow arrowheads in (E–E''') point to photoconverted *nkx2.5:*Kaede+ Isl1+ *myl7:*Cerulean+ pacemaker cardiomyocytes. White arrows in (G), (J–J'''), (L), and (O–O''') point to photoconverted *nkx2.5:*Kaede cells. Green, (G and L) non-photoconverted *nkx2.5:*Kaede; red, (B, D, E, E', G, I, J, J', L, N, O, and O') photoconverted *nkx2.5:*Kaede; cyan, (D, E, E'', I, J, J'', N, O, and O'') anti-Isl1 immunostaining; white, (D, E, E''', I, J, J''', N, O, and O''') anti-Nkx2.5 immunostaining; and blue, (D, E, I, J, N, and O) *myl7*:Cerulean. (P) Quantification of the localized photoconversion studies reveal that 14 ss *nkx2.5:*Kaede cells photoconverted at the most lateral edge of the *nkx2.5*+ mesoderm contribute primarily to pacemaker cardiomyocytes (red bar) along with a few atrial cardiomyocytes (green bar), whereas those photoconverted at the medial edge mainly supply ventricular cardiomyocytes (blue bar). (Q) Table summarizes the results of localized *nkx2.5:*Kaede photoconversion studies at the lateral (n = 55 cells from 24 embryos) and medial edge (n = 36 cells from 8 embryos). At, atrium and V, ventricle. Scale bar, 50 μm. See also Figure S1.

Because these fate-mapping studies suggest a dynamic role for Nkx2.5 during pacemaker CM formation, we further examined the developmental window in which Nkx2.5 may influence their development. Using the *Tg(hsp70l:nkx2.5-EGFP)* [or *Tg(hsp70:nkx2.5)*] line, we discovered that heat-shock (HS) induction of Nkx2.5 at 16 ss but not at 3, 10, or 23 ss, results in reduced pacemaker CM formation (Figures S1A–S1I'' and S1L–S1O), suggesting that decreasing Nkx2.5 expression in Nkx2.5+ cardiac progenitors between 16 and 23 ss is crucial for pacemaker CM development. Supporting these findings, we conversely observed that *nkx2.5*$^{-/-}$ mutants display increased Isl1+/*myl7:*eGFP+ pacemaker CMs at the atrial inflow tract region (Figures S1J–S1K'' and S1P), as

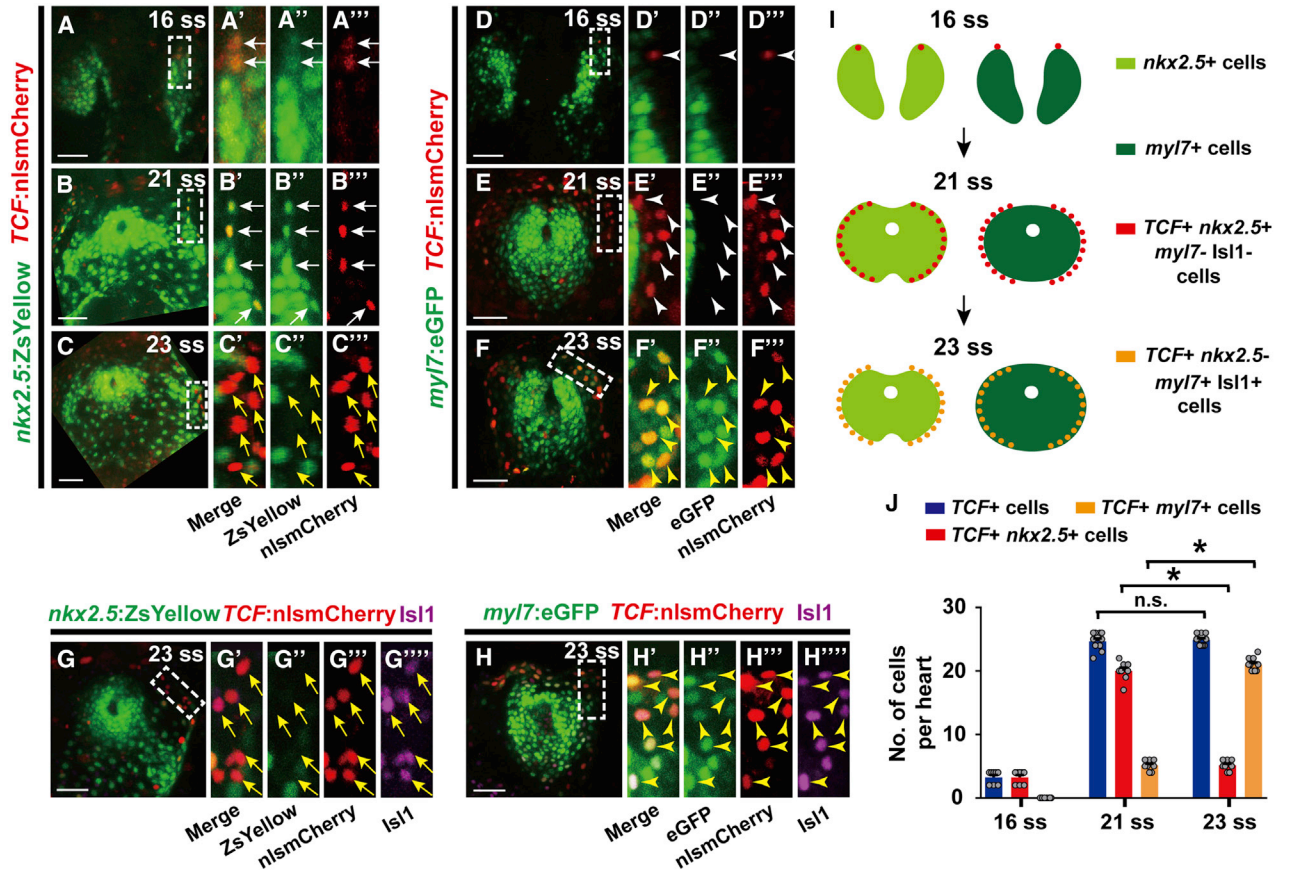

Figure 2. Nkx2.5 Expression Is Silenced While Canonical Wnt Signaling Is Activated in *nkx2.5*+ Progenitors during Pacemaker Cardiomyocyte Differentiation

(A–F''') Confocal images of (A–C''') *Tg(nkx2.5:ZsYellow; TCF:nlsmCherry)* (n = 8 embryos per stage) or (D–F''') *Tg(myl7:eGFP; TCF:nlsmCherry)* embryos (n = 8, 8, and 10 embryos for each respective stage) at (A–A''' and D–D''') 16, (B–B''' and E–E''') 21, or (C–C''' and F-F''') 23 ss reveal that canonical Wnt signaling is activated in outlying Nkx2.5+ mesodermal cells, which are decreasing *nkx2.5*:ZsYellow and increasing *myl7*:eGFP expression. (G–H'''') Anti-Isl1 immunostaining of (G–G'''') *Tg(nkx2.5:ZsYellow; TCF:nlsmCherry)* (n = 9 embryos) and (H–H'''') *Tg(myl7:eGFP; TCF:nlsmCherry)* (n = 10 embryos) embryos at 23 ss shows that canonical Wnt signaling (*TCF*:nlsmCherry+) is activated in *nkx2.5*:ZsYellow− Isl1+ cells and *myl7*:eGFP+ Isl1+ cardiomyocytes. (A'–A''', B'–B''', C'–C''', D'–D''', E'–E''', F'–F''', G'–G'''', and H'–H'''') Insets are magnifications of boxed areas in (A), (B), (C), (D), (E), (F), (G), and (H), respectively. Images in (A'' and A'''), (B'' and B'''), (C'' and C'''), (D'' and D'''), (E'' and E'''), (F'' and F'''), (G'' and G''''), and (H'' and H'''') are single channels from (A'), (B'), (C'), (D'), (E'), (F'), (G'), and (H') merged images, respectively. (I) Schematics based on (A–H'''') illustrate the dynamic changes in expression of *nkx2.5*:ZsYellow, *myl7*:eGFP, Isl1, and canonical Wnt-activation (*TCF*:nlsmCherry+) during pacemaker cardiomyocyte differentiation. (J) Further supporting these changes, quantification of *TCF*:nlsmCherry+ cells, *TCF*:nlsmCherry+ *nkx2.5*:ZsYellow+ cells, and *TCF*:nlsmCherry+ *myl7*:eGFP+ cardiomyocytes (per heart) at 16, 21, and 23 ss reveals that *TCF*:nlsmCherry+ *nkx2.5*:ZsYellow+ cells are significantly reduced while *TCF*:nlsmCherry+ *myl7*:eGFP+ cardiomyocytes are greatly increased from 21 to 23 ss. However, the total number of *TCF*:nlsmCherry+ cells is not changed. White arrows point to *TCF*:nlsmCherry+ *nkx2.5*:ZsYellow+ cells. Yellow arrows point to *TCF*:nlsmCherry+ *nkx2.5*:ZsYellow- cells. White arrowheads point to *TCF*:nlsmCherry+ *myl7*:eGFP− cells. Yellow arrowheads point to *TCF*:nlsmCherry+ *myl7*:eGFP+ cardiomyocytes. Green, (A–A'', B–B'', C–C'', and G–G'') *nkx2.5*:ZsYellow and (D–D'', E–E'', F–F'', and H–H'') *myl7*:eGFP; red, (A, A', A''', B, B', B''', C, C', C''', D, D', D''', E, E', E''', F, F', F''', G, G', G''', H, H', and H''') *TCF*:nlsmCherry; magenta, (G, G', G'''', H, H', and H'''') anti-Isl1 immunostaining. Scale bar, 50 μm. Mean ± SEM. *p < 0.05 by Student's t test. n.s., not significant. See also Figure S2.

recently reported (Colombo et al., 2018). Altogether, these Nkx2.5 fate-mapping and genetic studies reveal that pacemaker CMs derive from Nkx2.5+ cardiac precursors located at the most lateral regions of the ALPM, and that their differentiation from these precursors involves the coordinated activation of Isl1 and silencing of Nkx2.5 during a critical stage of heart development.

Canonical Wnt5b Signaling Directs Nkx2.5+ Progenitors to Pacemaker CMs

Based on these findings, we next searched for signaling pathways that could assign cardiomyocyte-pacemaker fate to the lateral regions of Nkx2.5-expressing mesoderm during this developmental window. Utilizing the *Tg(7x T-cell factor (TCF)-Xla.Siam:nlsmCherry)* [or *Tg(TCF:nlsmCherry)*] line, which reports activated canonical Wnt signaling (Moro et al., 2012), we observed *TCF*:nlsmCherry Wnt reporter activity in the outlying regions of the cardiac mesoderm (Figures 2A–2F'''), where cardiac pacemaker precursors reside at a developmental time period (16–23 ss) that is distinct from when canonical Wnt signaling is initiated during the pre-gastrulation stage to form cardiac mesoderm (Figures S2A–S2B'') (Barrow et al., 2007; Liu et al., 1999; Ueno et al., 2007). At 16 and 21 ss, this *TCF*:nlsmCherry signal

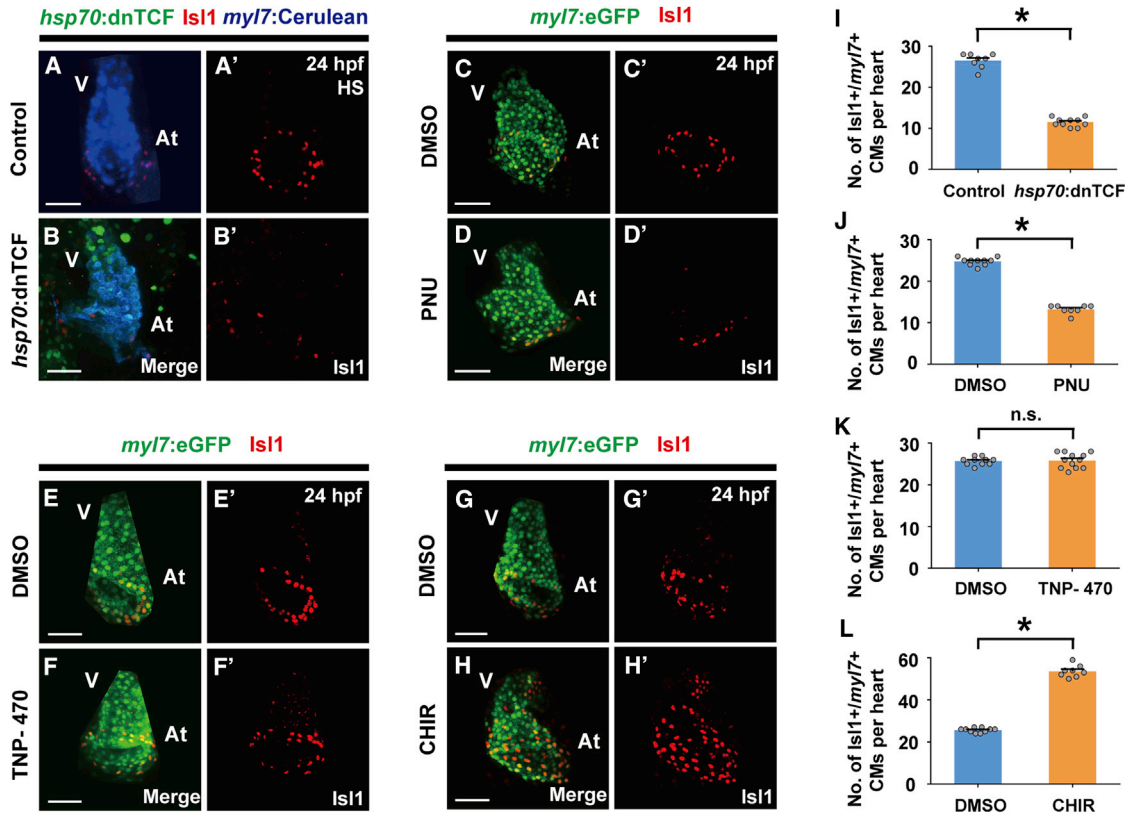

Figure 3. Canonical Wnt Signaling Is Required for Pacemaker-Cardiomyocyte Formation

Inhibiting canonical Wnt signaling by (B and B') heat-shock (HS) induction of *hsp70:*dnTCF (n = 10 embryos) or (D and D') PNU treatment (n = 8 embryos) at 16 ss reduces Isl1+/*myl7*+ pacemaker cardiomyocytes compared to (A and A') heat-shocked non-transgenic (n = 8 embryos) or (C and C') DMSO-treated controls (n = 10 embryos), respectively. However, inhibiting non-canonical Wnt signaling with (F and F') TNP-470 treatment (n = 12 embryos) has no discernible effect on pacemaker development, whereas activating canonical Wnt signaling with (H and H') CHIR (n = 8 embryos) at 16 ss promotes their expansion when compared to (E and E') and (G and G') respective DMSO controls (n = 10, 10 embryos). Images in (A'–H') are single channels from (A–H) merged images, respectively. Green, (B) *hsp70*:dnTCF and (C–H) *myl7*:eGFP; red, (A–H') anti-Isl1 immunostaining; and blue, (A and B) *myl7*:Cerulean. (I–L) Bar graphs show the number of Isl1+/*myl7*+ pacemaker cardiomyocytes (CMs) per heart for conditions in (A–B'), (C–D'), (E–F'), and (G–H'), respectively. At, atrium and V, ventricle. Scale bar, 50 μm. Mean ± SEM. *p < 0.05 by Student's t test. n.s., not significant. See also Figures S3–S5 and Tables S1 and S2.

co-localizes with *nkx2.5:*ZsYellow+ cardiac precursors but not differentiated *myl7:*eGFP+ cardiomyocytes (Figures 2A–2B''', white arrows; 2D–2E''',white arrowheads; 2I; and 2J). However, by 23 ss, this outlying canonical Wnt activity is primarily activated in *myl7*:eGFP+ cardiomyocytes that express the cardiac pacemaker marker Isl1 but not in *nkx2.5:*ZsYellow+ cells (Figures 2C–2C''' and 2G–2G'''', yellow arrows; 2F–2F''' and 2H–2H'''', yellow arrowheads; 2I and 2J), supporting a model in which canonical Wnt signaling is reactivated at this cardiac developmental stage to direct the differentiation of Nkx2.5+ cardiac precursors into pacemaker CMs expressing Isl1 and *myl7*:eGFP (a marker for differentiated cardiomyocytes) but not Nkx2.5. Thus, to explore this possibility, we investigated whether altering canonical Wnt activity during this period of heart development (16–23 ss) could affect the formation of pacemaker CMs. Using the *Tg(hsp70:dnTCF-GFP)* [or *Tg*(*hsp70:dnTCF*)] line, which can conditionally block canonical Wnt signaling through HS induction of dominant-negative TCF (dnTCF), or the canonical Wnt signaling chemical inhibitor PNU-74654 (PNU), we discovered that silencing canonical Wnt signaling at 16 ss leads to reduced pacemaker CMs as detected by decreased Isl1+/*myl7*:eGFP+ cardiomyocytes (Figures 3A–3D', 3I, and 3J) and diminished expression of *isl1*, *tbx18*, *shox2*, and *hcn4* genes at 48 hpf, when these genes together mark pacemaker CMs in the cardiac inflow tract region (Figures S3A–S3B''' and S4A–S4B''') (Birket et al., 2015; Liang et al., 2015; Mommersteeg et al., 2007; Protze et al., 2017; van Weerd and Christoffels, 2016; Wiese et al., 2009). However, treating embryos with TNP-470, an inhibitor of β-catenin-independent non-canonical Wnt activation, at 16 ss has no appreciable effect on pacemaker CM formation (Figures 3E–3F′, 3K, and S4E–S4F'''), further suggesting that Wnt signaling acts specifically through canonical pathways to control pacemaker CM development. In support of these findings, constitutively activated canonical Wnt signaling in either zebrafish embryos treated with the glycogen synthase kinase 3 inhibitor CHIR99021 (CHIR) at 16 ss (Figures 3G–3H′ and 3L) or *apc*^{sd58} mutant embryos (Figures 4A–4E′, 4F–4G′, and 4J) results in increased pacemaker CM formation including in the ventricle, but no effect on overall cardiomyocyte numbers (Figures 4H, 4I, and 4K), suggesting that these ectopic pacemaker CMs may develop at the expense of chamber cardiomyocytes. Consistent with this notion, hearts with constitutively activated Wnt signaling display an expansion of *isl1*, *tbx18*,

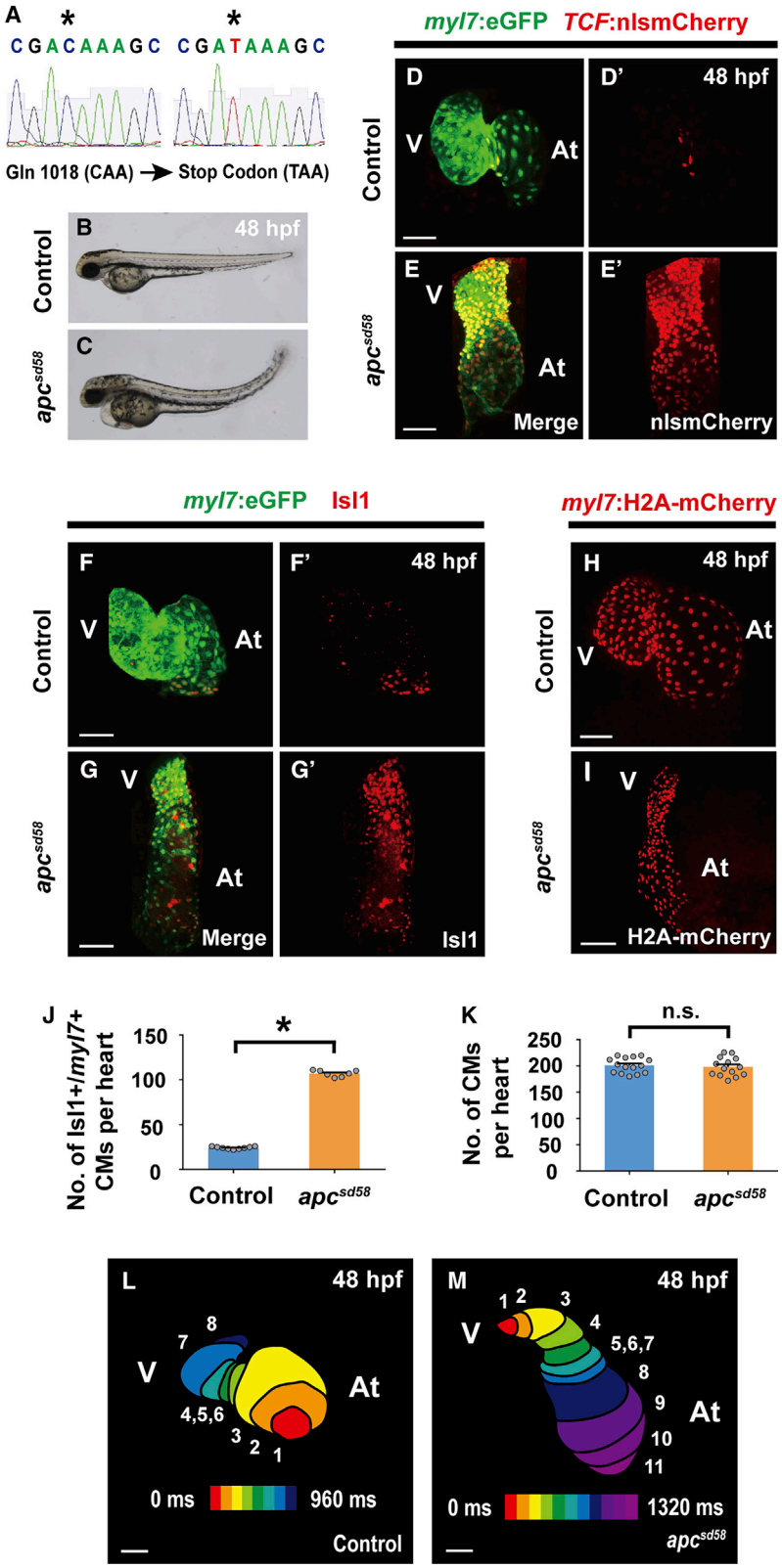

Figure 4. *apc* Loss-Of-Function Mutant (apc^{sd58}) Displays Constitutively Activated Canonical Wnt Signaling and Ectopic Pacemaker Formation

(A) Sequence analysis of *sd58* mutants reveals a C to T nonsense mutation at amino acid 1,018 in the *apc* gene, thus resulting in a putative premature truncation. (B and C) Bright-field microscopy of the lateral view of (B) wild-type (n = 12 embryos) and (C) apc^{sd58} mutant (n = 10 embryos) embryos shows that apc^{sd58} mutants display an upward curved tail and edema at 48 hpf. Confocal images of (D, D', F, F', and H) wild-type and (E, E', G, G', and I) apc^{sd58} mutant embryos at 48 hpf reveal that apc^{sd58} mutant hearts display (E and E') increased canonical Wnt-activation as detected by *TCF*:nlsmCherry (n = 8 embryos) and (G and G') increased number of Isl1+/*myl7*+ pacemaker cardiomyocytes (n = 7 embryos) but (I) no appreciable change in overall cardiomyocyte numbers (n = 14 embryos) when compared to (D, D', F, F', and H) respective wild-type control hearts (n = 7, 9, and 15 embryos). Images in (D'–G') are single channels from (D–G) merged images, respectively. Green, (D–G) *myl7*:eGFP and red, (D–E') *TCF*:nlsmCherry, (F–G') anti-Isl1 immunostaining, and (H and I) *myl7*:H2A-mCherry. (J and K) Bar graphs show the average number of (J) Isl1+/*myl7*+ pacemaker cardiomyocytes (CMs) from (F–G') or (K) total cardiomyocytes from (H and I). (L and M) Optical-mapping of the propagation of calcium activation in (L) control (n = 9 embryos) and (M) apc^{sd58} mutant (n = 7 embryos) hearts at 48 hpf reveals retrograde cardiac conduction from ventricle to atrium in apc^{sd58} mutants. Numbers at each isochronal line (60-ms intervals) indicate temporal sequence of calcium activation in the heart. At, atrium and V, ventricle. Scale bar, 50 μm. Mean ± SEM. *p < 0.05 by Student's t test. n.s., not significant. See also Figure S3.

shox2, and *hcn4* (Figures S3C–S3D''' and S4C–S4D'''). Confirming that these ectopic pacemaker CMs exhibit cardiac pacing capabilities, we discovered, by analyzing the propagation of cardiac excitation using the *Tg(myl7:gCaMP)* myocardial-specific calcium indicator line that *apc*^{sd58} mutant hearts harboring pacemaker CMs within the ventricle display retrograde cardiac conduction from the ventricular to the atrial chamber at 48 hpf (Figures 4L and 4M) when cardiac conduction typically propagates from atrium to ventricle in wild-type zebrafish embryos (Arrenberg et al., 2010; Chi et al., 2008). Finally, chromatin immunoprecipitation (ChIP) studies reveal that the β-catenin-TCF complex can interact with both Isl1 and Tbx18 enhancers harboring TCF-lymphoid enhancer-binding factor (LEF) binding sites (Figure S5), suggesting a possible mechanism by which Wnt signaling may initiate pacemaker differentiation. Overall, these findings support the conclusion that in addition to its previously reported cardiac developmental roles in inducing cardiac mesoderm formation during pre-gastrulation (Barrow et al., 2007; Liu et al., 1999; Ueno et al., 2007) and promoting the specification and expansion of SHF progenitors, which also prevents their differentiation into cardiomyocytes (Ai et al., 2007; Cohen et al., 2007; Kwon et al., 2007, 2009; Lin et al., 2007; Qyang et al., 2007), canonical Wnt signaling is redeployed in the outlying cardiac mesoderm from 16 to 23 ss to direct the differentiation of cardiac precursors into pacemaker CMs.

To identify potential Wnt ligands responsible for controlling pacemaker CM differentiation, we examined the expression of known Wnt ligands by *in situ* hybridization during heart development and discovered that *wnt5b* is expressed in a distribution similar to that of Wnt-activated cardiac precursors fated to become pacemaker CMs from 16 to 23 ss (Figures 5A–5C), and furthermore co-localizes with *nkx2.5:*ZsYellow+ cardiac precursors at 16 ss (Figures 5D–5D′). Supporting a role for Wnt5b in pacemaker CM development, we discovered that *wnt5b* loss-of-function (*ppt*) embryos exhibit fewer *TCF*:nlsmCherry+ cardiac precursors at the outlying regions of the cardiac mesoderm (Figures 5E–5G), a subsequent reduction in pacemaker CMs (Figures 5H–5J) including decreased *isl1*, *tbx18*, *shox2*, and *hcn4* pacemaker gene expression in the cardiac inflow tract (Figures S3E–S3F'''), and a significantly reduced heart rate (Figure 5K). Consistent with our findings suggesting that canonical Wnt signaling may affect the decisions of cardiac precursors to choose between an atrial or pacemaker CM fate, *wnt5b* mutant embryos additionally display an increase in atrial cardiomyocytes but no significant differences in cardiomyocyte cell death or proliferation compared to developmentally stage-matched wild-type embryos (Figure S6). In contrast to these loss-of-function studies, we observed that overexpressing Wnt5b at 16 ss using the HS inducible *Tg(hsp70l:wnt5b-GFP)* [or *Tg(hsp70:wnt5b)*] line results in not only increased canonical Wnt signaling activation in the cardiac mesoderm as detected by *TCF*:nlsmCherry (Figures 5L–5N), but also subsequent ectopic pacemaker CM formation (Figures 5O–5Q) including expanded *isl1*, *tbx18*, *shox2*, and *hcn4* pacemaker gene expression throughout the heart (Figures S3G–S3H'''). Together with our findings that inhibition of the non-canonical Wnt pathway does not affect pacemaker CM formation (Figures 3E–3F′, 3K, and S4E–S4F'''), these results support a role for Wnt5b as a key Wnt ligand that activates canonical Wnt signaling in the outlying regions of Nkx2.5 cardiac mesoderm between 16 and 23 ss to control gene regulatory programs instructing pacemaker CM fate. Moreover, manipulating canonical Wnt5b signaling can lead to an exchange of fates within these Nkx2.5+ cardiac mesodermal progenitors, suggesting that although these progenitors may be specified to become distinct cardiomyocyte lineages (Yelon et al., 1999), they also maintain the plasticity to switch fates upon exposure to specific signaling cues.

Activating Canonical Wnt Signaling in hPSCs Promotes Pacemaker-like Cardiomyocyte Differentiation

To explore whether these developmental concepts may be applied to hPSCs to create pacemaker CMs, we manipulated canonical Wnt signaling at the cardiac precursor stage during the differentiation of hPSCs into cardiomyocytes. Utilizing a highly efficient monolayer hPSC cardiac differentiation protocol (Lian et al., 2012), we initially differentiated H9 hPSCs harboring the *TNNT2:GFP* cardiac-specific transgene to an early *NKX2.5*-expressing cardiac precursor stage (day 5 - D5) (Lian et al., 2012) that corresponds to ~14–16 ss in the zebrafish through activating canonical Wnt signaling from D0 to D1, and then inhibiting it from D3 to D5 (Figures 6A and 6B). Similar to the *in vivo* zebrafish studies, canonical Wnt signaling was then re-activated in these hPSC cardiac precursors on D5 by treating them with the small molecule inhibitor CHIR (Figure 6A). Although this canonical Wnt signaling re-activation modestly reduces overall hPSC-cardiomyocyte differentiation efficiency (Figures 6C and 6D), it notably results in *TNNT2:*GFP+ hPSC-cardiomyocytes displaying pacemaker-like features (Figures 6E–6K, 6N–6Q, and 7) and expressing *BMP4* (Figure 6E), which has also been recently reported to promote pacemaker CM differentiation (Protze et al., 2017). These Wnt-activated hPSC-cardiomyocytes, which express the cardiomyocyte marker TNNT2, exhibit not only significantly elevated expression of pacemaker-related genes *SHOX2*, *HCN4*, *ISL1*, *TBX3*, and *TBX18* but also a corresponding decrease in *NKX2.5* expression (Figures 6F–6K), which were confirmed by SHOX2 and NKX2.5 immunostaining (Figures 6N–6Q). In line with these studies, hPSC cardiac precursors treated with WNT5B from D5 to D7 furthermore display significantly increased expression of pacemaker-related genes and decreased expression of *NKX2.5* (Figure S7). Functionally supporting these findings, single-cell patch clamping studies further revealed that while control (DMSO treated) cardiomyocytes primarily display action potentials (APs) observed in chamber cardiomyocytes including a more consistent and negative resting membrane potential than pacemaker CMs (Figures 7A and 7C), Wnt-activated hPSC-cardiomyocytes exhibit pacemaker-like APs with less negative resting membrane potentials (Figures 7B and 7C). Corresponding with this change to pacemaker-like characteristics, these Wnt-activated hPSC-cardiomyocytes also display significantly faster beating rates than those detected in control hPSC-cardiomyocytes (Figure 7D), corroborating their increased automaticity. Thus, these molecular and cellular findings support that hPSC-cardiomyocytes, which derive from cardiac precursors where Wnt signaling is re-activated during a critical window of cardiomyocyte differentiation, exhibit key features of pacemaker CMs that distinguish them from cardiac progenitor cells, including the presence and absence of a combination of genes

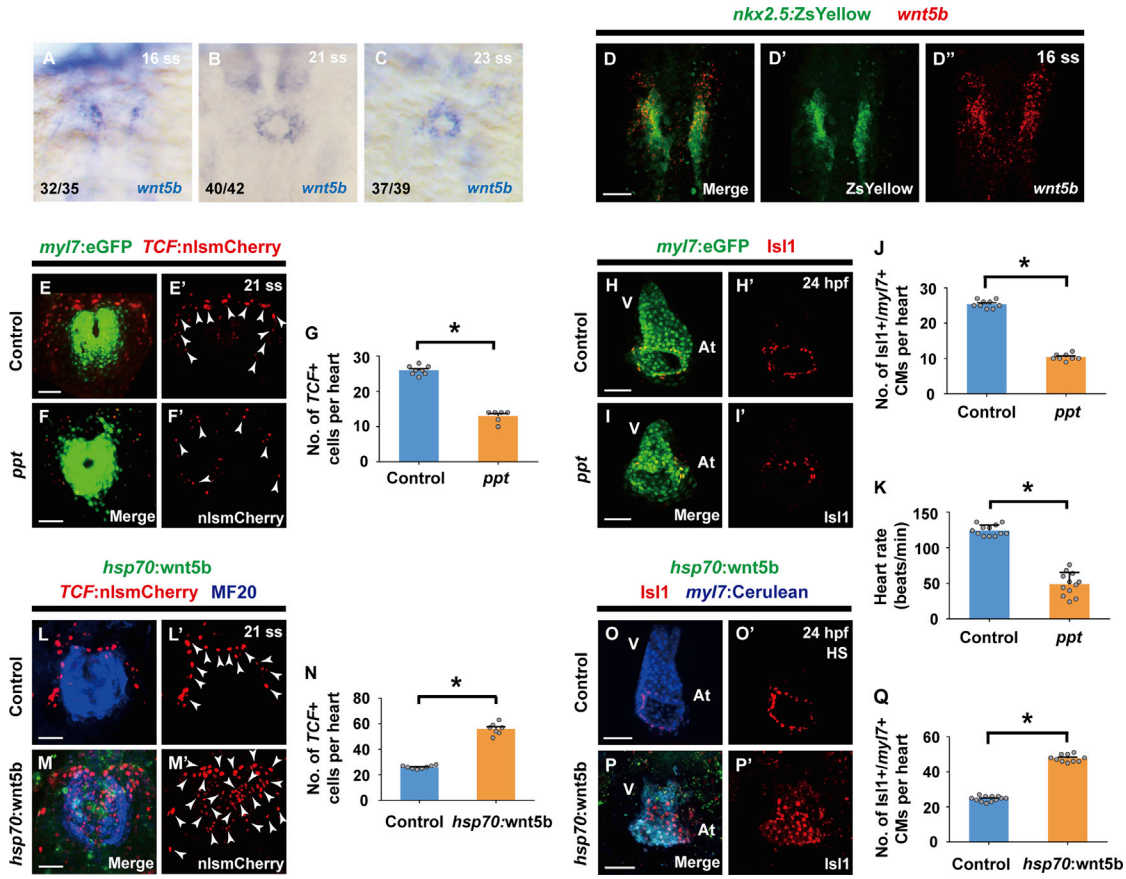

Figure 5. Wnt5b Is Required for Canonical Wnt Activation during Pacemaker-Cardiomyocyte Development

(A–C) *In situ* hybridization analyses reveals *wnt5b* expression within the ALPM at (A) 16 ss as well as in the cardiac mesoderm at (B) 21 ss and (C) 23 ss. (D–D'') *wnt5b* RNAscope *in situ* hybridization in *Tg(nkx2.5:ZsYellow)* wild-type embryos (n = 12 embryos) shows that there is an overlap in *nkx2.5:*ZsYellow and *wnt5b* expression at 16 ss. (E–F' and H–I') Confocal images of (E–F') *Tg(myl7:eGFP; TCF:nlsmCherry)* (E and E') wild-type control (n = 8 embryos) or (F and F') *ppt* mutant embryos (n = 6 embryos) at 21 ss and (H–I') anti-Isl1 immunostaining of *Tg(myl7:eGFP)* (H and H') wild-type control (n = 9 embryos) or (I and I') *ppt* mutant embryos (n = 8 embryos) at 24 hpf show that loss of *wnt5b* (*ppt*) leads to less *TCF*:nlsmCherry+ cells in the outlying regions of the cardiac mesoderm and subsequently fewer Isl1+/*myl7*+ pacemaker cardiomyocytes at the inflow tract region. Conversely, overexpressing *wnt5b* by (M and M') and (P and P') heat-shocking *Tg(hsp70:wnt5b)* embryos (n = 7 and 10 embryos) at 16 ss results in increased *TCF*:nlsmCherry+ cells in the cardiac mesoderm at 21 ss and increased Isl1+/*myl7*+ pacemaker cardiomyocytes at the inflow tract region at 24 hpf compared to (L–L' and O–O') non-transgenic heat-shocked sibling controls (n = 8, 12 embryos). Images in (D'), (D''), (E'), (F'), (H'), (I'), (L'), (M'), (O'), and (P') are single channels from (D), (E), (F), (H), (I), (L), (M), (O), and (P) merged images, respectively. Green, (D and D') *nkx2.5*:ZsYellow, (E, F, H, and I) *myl7*:eGFP, (M and P) *hsp70:*wnt5b; red, (D and D'') *wnt5b* RNAscope *in situ* hybridization probe, (E and F' and L–M') *TCF*:nlsmCherry, (H–I' and O–P') anti-Isl1 immunostaining; blue, (L and M) anti-MF20 immunostaining, (O and P) *myl7*:Cerulean. White arrowheads point to *TCF*:nlsmCherry+ cells. (G, J, N, and Q) Bar graphs show the average number of (G and N) *TCF*:nlsmCherry+ cells per heart for conditions in (E–F') and (L–M') and (J and Q) Isl1+/*myl7*+ pacemaker cardiomyocytes (CMs) per heart for conditions in (H–I') and (O–P'), respectively. (K) Bar graph shows the heart rate for wild-type control (n= 12 embryos) and *ppt* mutant embryos (n= 12 embryos) at 48 hpf. For *in situ* hybridization studies in (A–C), ratios indicate the number of embryos displaying the respective gene expression pattern versus total number of embryos analyzed. Scale bar, 50 μm. Mean ± SEM. *$p < 0.05$ by Student's t test. See also Figures S3 and S6.

specific to pacemaker CMs (*SHOX2*+, *HCN4*+, *ISL1*+, *TBX3*+, *TBX18*+, but *NKX2.5*−) (Birket et al., 2015; Liang et al., 2015; Mommersteeg et al., 2007; Protze et al., 2017; van Weerd and Christoffels, 2016; Wiese et al., 2009), their differentiation into cardiomyocytes expressing TNNT2, and their electrophysiologic attributes promoting enhanced cardiac automaticity. Finally, consistent with recent studies showing that temporal modulation of canonical Wnt signaling may induce epicardial cell formation in hPSCs (Bao et al., 2016; Iyer et al., 2015), we notably also found that hPSC *TNNT2*:GFP-negative non-cardiomyocyte cells derived from these Wnt re-activated hPSC cardiac precursors exhibit significantly increased expression of the epicardial marker genes *TBX18*, *WT1*, and *TCF21* but decreased expression of *NKX2.5* (Figures 6J–6M).

Canonical Wnt-Activated hPSC Pacemaker-like Cardiomyocytes Can Pace *In Vitro* Bioprinted Mini Heart Models

Employing a rapid 3D bioprinting technology to create *in vitro* multi-cellular cardiac models (Figure 7F), we next investigated whether these Wnt-activated hPSC-pacemaker-like cardiomyocytes could functionally pace *in vitro* prefabricated cardiac tissues composed of hPSC-cardiomyocytes. To this end, we bioprinted purified hPSC-cardiomyocytes into a heart-shape

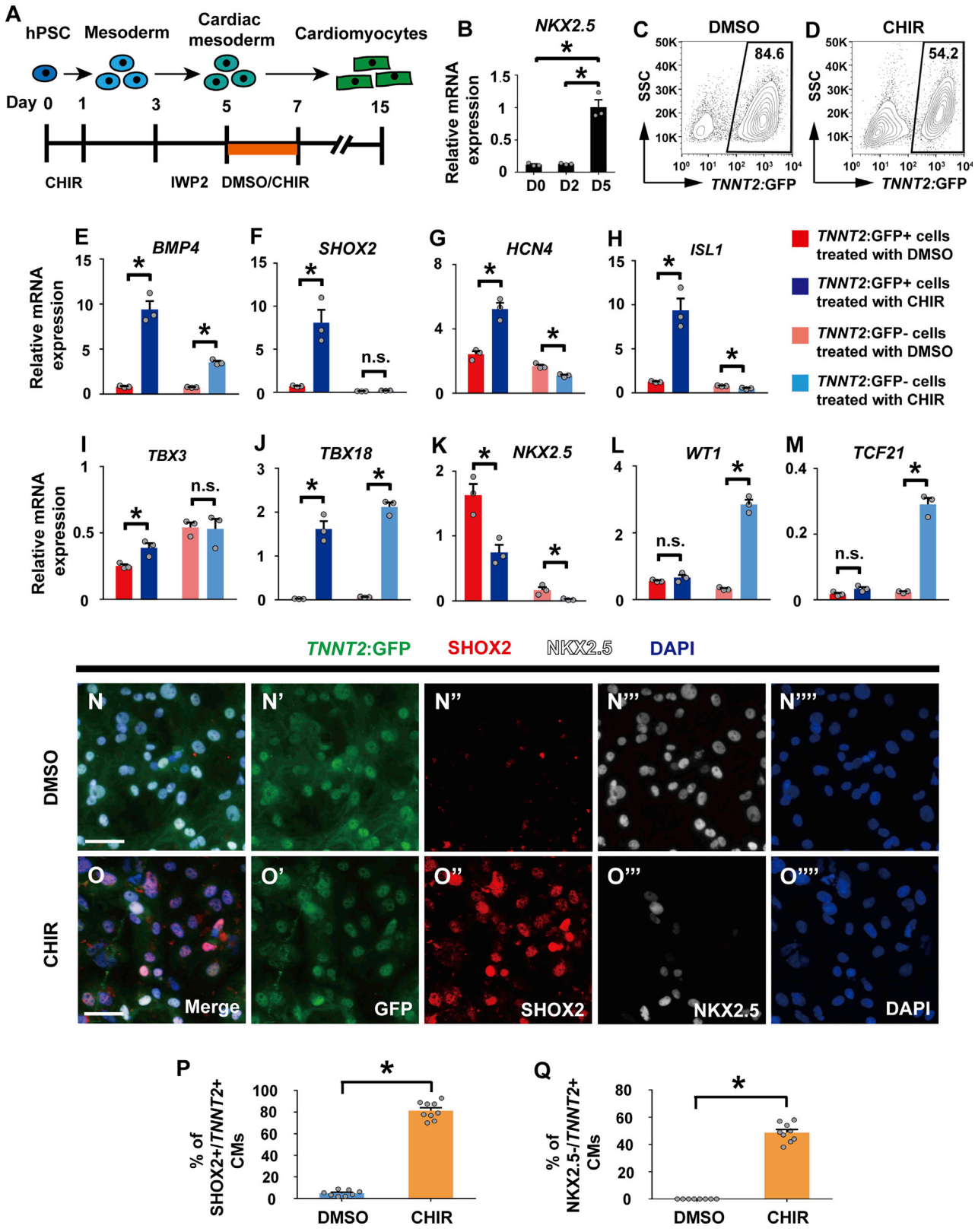

(legend on next page)

configuration (i.e., "mini hearts") with a gap in the upper left region (Figures 7G, 7H, 7J, and 7K). Within this excluded area, we then immediately bioprinted either purified control (DMSO) or Wnt-activated hPSC-cardiomyocytes (Figures 7G, 7H, 7J, and 7K, dashed circle) to examine whether Wnt-activated hPSC-cardiomyocytes specifically display pacemaker activity that can pace the bioprinted hPSC-cardiomyocyte tissues. After confirming recovery and re-synchronization of these bioprinted cardiomyocytes, we then performed optical-mapping analyses using calcium imaging on these mini hearts. In contrast to mini hearts with bioprinted control hPSC-cardiomyocytes, which display randomly initiated electrical activity (Figure 7I; Video S1), mini hearts with Wnt-activated hPSC-cardiomyocytes consistently initiate cardiac electrical activity from the upper left region (Figure 7L; Video S2) and exhibit faster paced beating rates (Figure 7E; Videos S3 and S4). Altogether, these results reveal that activating canonical Wnt signaling in hPSC-derived cardiac progenitors can initiate the gene regulatory program that directs their differentiation into human pacemaker-like cardiomyocytes that are capable of pacing human cardiac tissue.

DISCUSSION

Overall, through identifying the origins of pacemaker CMs, we discovered that Wnt5b functions as an inductive signaling cue that activates a conserved canonical Wnt signaling pathway, which instructs the fate of Nkx2.5+ cardiac progenitors into the cardiac pacemaker lineage. Although previous studies suggest that pacemaker CMs may derive from mesodermal progenitor cells not expressing Nkx2.5 (Bressan et al., 2013), our fate-mapping studies reveal that they can originate from Nkx2.5+ cardiac precursors, which are specifically located adjacent but also lateral to Nkx2.5+ cardiac mesoderm fated to become atrial cardiomyocytes as suggested in recent mouse studies (Mommersteeg et al., 2010). Consistent with these mouse studies, we further observed Wnt-mediated dynamic silencing of Nkx2.5 during pacemaker CM differentiation, which may explain the recent findings suggesting that pacemaker CMs may derive from cardiac mesoderm not expressing Nkx2.5 (Bressan et al., 2013). However, our studies do not preclude the possibility that given the heterogeneity of cells composing the sinoatrial node (Liang et al., 2015; Sun et al., 2007), pacemaker CMs may derive from multiple cardiac progenitor cell sources.

Canonical Wnt signaling has been reported to regulate multiple aspects of cardiac development, including the induction of cardiac mesoderm formation during pre-gastrulation (Barrow et al., 2007; Liu et al., 1999; Ueno et al., 2007) and the specification and expansion of SHF cardiac progenitor cells at later stages, where canonical Wnt also prevents their differentiation into cardiomyocytes (Ai et al., 2007; Cohen et al., 2007; Kwon et al., 2007, 2009; Lin et al., 2007; Qyang et al., 2007). In addition to mediating these cardiac developmental events, we have further discovered that canonical Wnt signaling is also redeployed to direct outlying Nkx2.5+ progenitors into pacemaker CMs. In contrast to its role for promoting the expansion of SHF cardiac progenitors and inhibiting their differentiation into cardiomyocytes (Ai et al., 2007; Cohen et al., 2007; Kwon et al., 2007, 2009; Lin et al., 2007; Qyang et al., 2007), we observed that canonical Wnt signaling, which promotes the differentiation of cardiac progenitors into pacemaker CMs, functions through not only the activation of a combination of well-established markers specific to pacemaker CMs (*SHOX2*, *ISL1*, *TBX18*, *HCN4*, and *TBX3*) (Birket et al., 2015; Liang et al., 2015; Mommersteeg et al., 2007; Protze et al., 2017; van Weerd and Christoffels, 2016; Wiese et al., 2009) but also the expression of cardiomyocyte differentiation markers (*myl7* in zebrafish and TNNT2 in hPSCs), which distinguishes these pacemaker CMs from cardiac progenitors.

Supporting an additional cardiac developmental role of canonical Wnt signaling in pacemaker CM differentiation that is distinct from its role in specification and expansion of cardiac progenitor cells, we discovered that the ligand responsible for controlling pacemaker CM differentiation is Wnt5b rather than Wnt3 and Wnt8, which have been reported to mediate cardiac progenitor cell formation (Barrow et al., 2007; Jaspard et al., 2000; Liu et al., 1999). Although Wnt5b has been observed to function primarily through non-canonical Wnt signaling pathways (Kilian et al., 2003; Merks et al., 2018), we discovered that similar to lymphatic developmental studies (Nicenboim et al., 2015), it can also induce canonical Wnt signaling in these Nkx2.5+ progenitor cells to both directly activate expression of Isl1 and Tbx18, which are transcriptional regulators involved in pacemaker CM differentiation (Kapoor et al., 2013; Liang et al.,

Figure 6. Activating Canonical Wnt Signaling in Human Pluripotent Stem Cell (hPSC)-Cardiac Progenitors Promotes Pacemaker-like Cardiomyocyte Differentiation

(A) Schematic illustrates the experimental design for inducing human pacemaker-like cardiomyocyte differentiation through activating canonical Wnt signaling in *TNNT2*:GFP hPSC-cardiac progenitors (i.e., adding 3 μM CHIR from D5–D7).

(B) *NKX2.5* expression was analyzed by qRT-PCR (n = 3 independent cardiomyocyte differentiations) for hPSCs differentiating into cardiomyocytes on D0, D2, and D5. Bar graphs represent average gene expression relative to the housekeeping gene TATA-box binding protein (*TBP*).

(C and D) After treating *TNNT2*:GFP hPSCs with (C) DMSO or (D) 3 μM CHIR during days 5–7 of the monolayer cardiomyocyte differentiation protocol, hPSC-cardiomyocyte differentiation was assessed at day 15 by flow cytometry (n = 3 independent differentiations).

(E–M) *TNNT2*:GFP+ and *TNNT2*:GFP− cells generated in (C) and (D) were sorted and then analyzed for (E) *BMP4*, (F) *SHOX2*, (G) *HCN4*, (H) *ISL1*, (I) *TBX3*, (J) *TBX18*, (K) *NKX2.5*, (L) *WT1*, and (M) *TCF21* expression by qRT-PCR (n = 3 independent differentiations). Bar graphs represent average gene expression relative to the housekeeping gene *TBP*.

(N–O'''') Confocal images of *TNNT2*:GFP+ cardiomyocytes sorted from D15 cultures and immunostained for SHOX2 and NKX2.5 reveal that treating hPSC-cardiac progenitors with (O–O'''') CHIR from D5–D7 (n = 3 independent differentiations) results in increased SHOX2+/*TNNT2*+ and NKX2.5-/*TNNT2*+ cardiomyocytes compared to (N–N'''') DMSO treatment from D5–D7 (n = 3 independent differentiations). Images in (N'–N'''') and (O'–O'''') are single channels from (N) and (O) merged images, respectively. Green, (N, N', O, and O') *TNNT2*:GFP; red, (N, N'', O, and O'') anti-SHOX2 immunostaining; white, (N, N''', O, and O''') anti-NKX2.5 immunostaining; and blue, (N, N'''', O, and O'''') DAPI.

(P and Q) Bar graphs show the percentage of (P) SHOX2+/*TNNT2*+ and (Q) NKX2.5−/*TNNT2*+ cardiomyocytes (CMs) for D5–D7 (N–N'''') DMSO (n = 8) or (O–O'''') CHIR (n = 9) treatment conditions. Scale bar, 50 μm. Mean ± SEM. *$p < 0.05$ by Student's t test. n.s., not significant. See also Figure S7 and Tables S1 and S3.

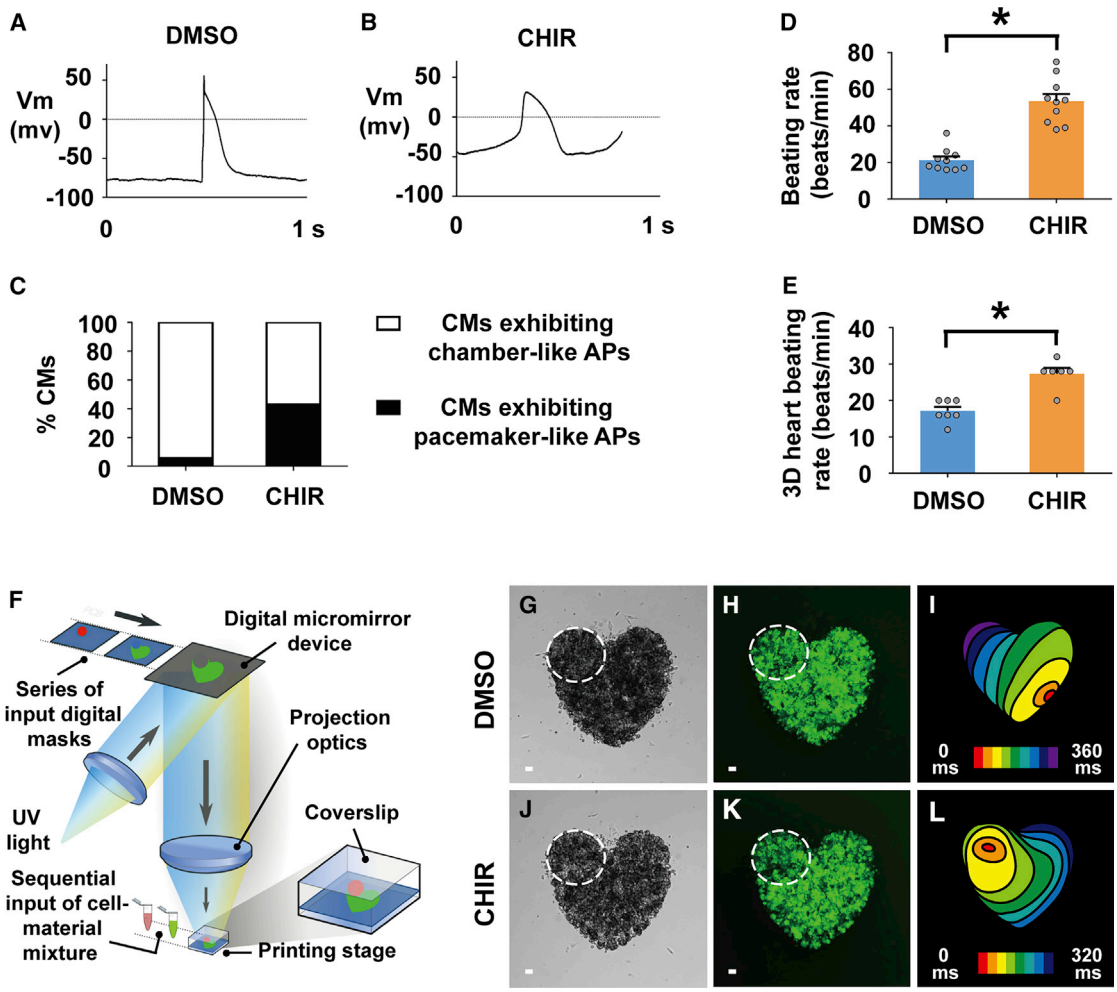

Figure 7. Activating Canonical Wnt Signaling in Human Pluripotent Stem Cell (hPSC)-Cardiac Progenitors Creates Functional Pacemaker-like Cardiomyocytes That Can Pace hPSC-Cardiomyocytes *In Vitro*

(A and B) Electrophysiology recordings reveal action potentials of individual cardiomyocytes sorted from D15 cultures which were treated with (A) DMSO (n = 18 cardiomyocytes) or (B) CHIR (n = 14 cardiomyocytes) from D5–D7.

(C) Electrophysiology studies on these *TNNT2:*GFP+ hPSC-cardiomyocytes (CMs) reveals that a greater percentage of CHIR-treated hPSC-cardiomyocytes (n = 14 cardiomyocytes) exhibit pacemaker-like action potentials (APs) than DMSO-treated hPSC-cardiomyocytes (n = 18 cardiomyocytes).

(D) Bar graph shows the average beating rate for cardiomyocytes sorted from D15 cultures that were exposed to either DMSO (n = 10 cardiomyocytes) or CHIR (n = 10 cardiomyocytes) treatment from D5–D7.

(E–L) hPSC-derived pacemaker-like cardiomyocytes can pace hPSC-cardiomyocyte tissue *in vitro*. (F) Diagram illustrates 3D bioprinting approach. (G–L) To create multi-cellular *in vitro* mini hearts, D15 hPSC-cardiomyocytes treated with (G and H) DMSO or (J and K) CHIR from D5–D7 are printed in the upper left region of mini hearts (dashed lines encircle area), and D15 hPSC-cardiomyocytes are printed outside this encircled region. (G and J) Bright-field and (H and K) GFP microscopy images show printed mini hearts. (I and L) Optical-mapping of the calcium activation in these mini hearts reveals that cardiac conduction is stably initiated from the site of printed (L) CHIR-treated pacemaker-like cardiomyocytes (n = 6 mini hearts) but not (I) DMSO-treated control cardiomyocytes (n = 7 mini hearts). Red-orange, cardiac conduction initiation site; isochronal lines, 40 milliseconds (ms) intervals. (E) Bar graph shows that the average beating rate is significantly faster in mini hearts printed with CHIR-treated pacemaker-like cardiomyocytes (n = 6 mini hearts) compared to those printed with DMSO-treated control cardiomyocytes (n = 7 mini hearts). Scale bar, 50 μm. Mean ± SEM. *$p < 0.05$ by Student's t test. See also Videos S1, S2, S3, and S4.

2015; Tessadori et al., 2012; Vedantham et al., 2015; Wiese et al., 2009), and inhibit Nkx2.5 expression likely through Isl1-activated expression of Shox2 (Liang et al., 2015; van Weerd and Christoffels, 2016), which has been reported to inhibit Nkx2.5 expression (Espinoza-Lewis et al., 2009). Moreover, our results suggest a role for Wnt5b in partitioning the outlying regions of the Nkx2.5+ cardiac progenitor pool between pacemaker and atrial cardiomyocyte fates, as perturbing Wnt5b activity alters the contributions of these cardiomyocyte cell types to the developing heart. Given that Wnt5b can control Tbx18, which has been reported to regulate not only pacemaker CM (Kapoor et al., 2013; Wiese et al., 2009) but also epicardial cell development (Cai et al., 2008; Christoffels et al., 2009), future investigations into Wnt5b may illuminate whether it also regulates the development of other cardiovascular cell types arising from the outlying domains of the heart fields (Bressan et al., 2013). In line with this possibility, we discovered that temporally activating canonical Wnt signaling during hPSC-cardiomyocyte differentiation not

only produced TNNT2+ pacemaker CMs but also TNNT2-negative epicardial cells, which is consistent with recent hPSC epicardial cell differentiation studies (Bao et al., 2016; Iyer et al., 2015).

Finally, supporting that this canonical Wnt signaling pathway is evolutionarily conserved during pacemaker cell differentiation, these developmental principles can be applied to hPSC cardiac precursors to direct their differentiation into pacemaker-like cardiomyocytes that are able to pace other hPSC-cardiomyocytes. Similar to recent hPSC cardiac pacemaker differentiation studies (Birket et al., 2015; Protze et al., 2017), our studies utilize an early inhibition of Wnt signaling to promote cardiac progenitor cell specification. In contrast to these studies that report coordinated manipulation of several signaling pathways (including BMP and retinoic acid (RA) activation and fibroblast growth factor (FGF) inhibition) to create pacemaker-like cardiomyocytes (Birket et al., 2015; Protze et al., 2017), we discovered that re-activation of Wnt signaling in these cardiac progenitor cells is sufficient to promote the differentiation of cardiac precursors into pacemaker-like cardiomyocytes that express a similar combination of pacemaker genes (*SHOX2*+, *HCN4*+, *ISL1*+, *TBX3*+, *TBX18*+, but *NKX2.5*−), which have been previously reported in other hPSC pacemaker CM studies (Birket et al., 2015; Protze et al., 2017) or overexpressed *in vivo* to convert existing working cardiomyocytes into pacemaker-like cells (Bakker et al., 2012; Hoogaars et al., 2007; Kapoor et al., 2013). Supporting that canonical Wnt signaling may promote pacemaker CM differentiation through regulating BMP signaling, we notably observed that this redeployment of canonical Wnt signaling does lead to a substantial increase in the expression of *BMP4*, which has been reported as a key signal to direct not only cardiac pacemaker cell differentiation in these hPSC pacemaker studies (Protze et al., 2017) but also hPSC epicardial cell differentiation (Witty et al., 2014). Although these complementary findings appear to differ from recent hPSC reports suggesting BMP and FGF inhibition promote pacemaker CM differentiation (Birket et al., 2015), these discrepancies may be due to the timing and coordination of signaling pathways that regulate pacemaker CM differentiation. Overall, our findings support a model in which canonical Wnt signaling is redeployed during cardiac development to mediate the specification of cardiac pacemaker cells through coordinating a hierarchical signaling cascade, which may include BMP signaling and other signaling pathways (FGF and RA) that not only direct cardiac progenitor cells toward cardiac pacemaker fates but also prevent them from differentiating into other cardiomyocyte cell types.

STAR★METHODS

Detailed methods are provided in the online version of this paper and include the following:

- KEY RESOURCES TABLE
- LEAD CONTACT AND MATERIALS AVAILABILITY
- EXPERIMENTAL MODEL AND SUBJECT DETAILS
  - Animals
  - Human Pluripotent Stem Cells
- METHOD DETAILS
  - Nkx2.5 Photoconversion Studies
  - Heat Shock Induction and Small Molecule Inhibitor Studies in Zebrafish
  - *In Situ* Hybridization, Immunofluorescence, TUNEL Assays in Zebrafish
  - RNAscope *In Situ* Hybridization
  - Optical Mapping for Zebrafish Embryos
  - Chromatin Immunoprecipitation (ChIP) Studies
  - Human Pluripotent Stem Cell (hPSC) Studies
  - Electrophysiology
  - 3D Bioprinting and Optical Mapping of hPSC-Derived Cardiomyocyte "Mini Hearts"
  - Cardiomyocyte Beating Rate Analysis
- QUANTIFICATION AND STATISTICAL ANALYSIS
- DATA AND CODE AVAILABILITY

SUPPLEMENTAL INFORMATION

Supplemental Information can be found online at https://doi.org/10.1016/j.devcel.2019.07.014.

ACKNOWLEDGMENTS

We thank N. Tedeschi for fish care; Z. Huang for experimental assistance; S.M. Evans, D. Yelon, and N.C. Chi lab members for comments on the manuscript; G. Crump and W. Herzog for plasmids; C.G. Burns for the Nkx2.5 photoconversion line; K.L. Targoff for the heat shock Nkx2.5 line; and F. Argenton for the canonical Wnt signaling reporter line. This work was supported in part by grants from the American Heart Association (15POST23090027) to J.R., the Saving Tiny Hearts Foundation and NIH (R01HL108599) to D.Y., CIRM (RT3-07899) and NIH (R01EB021857) to S.C., and NIH to N.C.C.

AUTHOR CONTRIBUTIONS

J.R. and N.C.C. conceived the project and the overall design of the experimental strategy. J.R., P.H., X.M., E.N.F., J.B., X.-X.I.Z., R.Z., M.M.S., A.D.W., H.G.K., R.D., and W.X. conducted the experiments. D.Y. helped in the design of zebrafish studies and provided key reagents including assistance with photoconversion studies. S.C. helped in designing and providing key reagents for the 3D bioprinting experiments. J.R., J.B., D.Y., and N.C.C. prepared the manuscript.

DECLARATION OF INTERESTS

The authors declare no competing interests.

Received: January 27, 2019
Revised: May 1, 2019
Accepted: July 11, 2019
Published: August 8, 2019

SUPPORTING CITATIONS

The following references appear in the Supplemental Information: Chen et al., 2014; Pradhan and Olsson, 2014.

REFERENCES

Ai, D., Fu, X., Wang, J., Lu, M.F., Chen, L., Baldini, A., Klein, W.H., and Martin, J.F. (2007). Canonical Wnt signaling functions in second heart field to promote right ventricular growth. Proc. Natl. Acad. Sci. USA *104*, 9319–9324.

Arrenberg, A.B., Stainier, D.Y., Baier, H., and Huisken, J. (2010). Optogenetic control of cardiac function. Science *330*, 971–974.

Bakker, M.L., Boink, G.J., Boukens, B.J., Verkerk, A.O., van den Boogaard, M., den Haan, A.D., Hoogaars, W.M., Buermans, H.P., de Bakker, J.M., Seppen, J., et al. (2012). T-box transcription factor TBX3 reprogrammes mature cardiac myocytes into pacemaker-like cells. Cardiovasc. Res. *94*, 439–449.

Bao, X., Lian, X., Hacker, T.A., Schmuck, E.G., Qian, T., Bhute, V.J., Han, T., Shi, M., Drowley, L., Plowright, A., et al. (2016). Long-term self-renewing human epicardial cells generated from pluripotent stem cells under defined xeno-free conditions. Nat. Biomed. Eng. *1*.

Barrow, J.R., Howell, W.D., Rule, M., Hayashi, S., Thomas, K.R., Capecchi, M.R., and McMahon, A.P. (2007). Wnt3 signaling in the epiblast is required for proper orientation of the anteroposterior axis. Dev. Biol. *312*, 312–320.

Birket, M.J., Ribeiro, M.C., Verkerk, A.O., Ward, D., Leitoguinho, A.R., den Hartogh, S.C., Orlova, V.V., Devalla, H.D., Schwach, V., Bellin, M., et al. (2015). Expansion and patterning of cardiovascular progenitors derived from human pluripotent stem cells. Nat. Biotechnol. *33*, 970–979.

Blaschke, R.J., Hahurij, N.D., Kuijper, S., Just, S., Wisse, L.J., Deissler, K., Maxelon, T., Anastassiadis, K., Spitzer, J., Hardt, S.E., et al. (2007). Targeted mutation reveals essential functions of the homeodomain transcription factor Shox2 in sinoatrial and pacemaking development. Circulation *115*, 1830–1838.

Bogdanovic, O., Fernandez-Miñán, A., Tena, J.J., de la Calle-Mustienes, E., Hidalgo, C., van Kruysbergen, I., van Heeringen, S.J., Veenstra, G.J., and Gómez-Skarmeta, J.L. (2012). Dynamics of enhancer chromatin signatures mark the transition from pluripotency to cell specification during embryogenesis. Genome Res. *22*, 2043–2053.

Bressan, M., Liu, G., and Mikawa, T. (2013). Early mesodermal cues assign avian cardiac pacemaker fate potential in a tertiary heart field. Science *340*, 744–748.

Bu, L., Jiang, X., Martin-Puig, S., Caron, L., Zhu, S., Shao, Y., Roberts, D.J., Huang, P.L., Domian, I.J., and Chien, K.R. (2009). Human ISL1 heart progenitors generate diverse multipotent cardiovascular cell lineages. Nature *460*, 113–117.

Cai, C.L., Liang, X., Shi, Y., Chu, P.H., Pfaff, S.L., Chen, J., and Evans, S. (2003). Isl1 identifies a cardiac progenitor population that proliferates prior to differentiation and contributes a majority of cells to the heart. Dev. Cell *5*, 877–889.

Cai, C.L., Martin, J.C., Sun, Y., Cui, L., Wang, L., Ouyang, K., Yang, L., Bu, L., Liang, X., Zhang, X., et al. (2008). A myocardial lineage derives from Tbx18 epicardial cells. Nature *454*, 104–108.

Cao, N., Huang, Y., Zheng, J., Spencer, C.I., Zhang, Y., Fu, J.D., Nie, B., Xie, M., Zhang, M., Wang, H., et al. (2016). Conversion of human fibroblasts into functional cardiomyocytes by small molecules. Science *352*, 1216–1220.

Cha, B., Geng, X., Mahamud, M.R., Fu, J., Mukherjee, A., Kim, Y., Jho, E.H., Kim, T.H., Kahn, M.L., Xia, L., et al. (2016). Mechanotransduction activates canonical Wnt/beta-catenin signaling to promote lymphatic vascular patterning and the development of lymphatic and lymphovenous valves. Genes Dev. *30*, 1454–1469.

Chen, E.Y., DeRan, M.T., Ignatius, M.S., Grandinetti, K.B., Clagg, R., McCarthy, K.M., Lobbardi, R.M., Brockmann, J., Keller, C., Wu, X., et al. (2014). Glycogen synthase kinase 3 inhibitors induce the canonical WNT/beta-catenin pathway to suppress growth and self-renewal in embryonal rhabdomyosarcoma. Proc. Natl. Acad. Sci. USA *111*, 5349–5354.

Chi, N.C., Shaw, R.M., Jungblut, B., Huisken, J., Ferrer, T., Arnaout, R., Scott, I., Beis, D., Xiao, T., Baier, H., et al. (2008). Genetic and physiologic dissection of the vertebrate cardiac conduction system. PLoS Biol. *6*, e109.

Christoffels, V.M., Grieskamp, T., Norden, J., Mommersteeg, M.T., Rudat, C., and Kispert, A. (2009). Tbx18 and the fate of epicardial progenitors. Nature *458*, E8–E9.

Christoffels, V.M., Mommersteeg, M.T., Trowe, M.O., Prall, O.W., de Gier-de Vries, C., Soufan, A.T., Bussen, M., Schuster-Gossler, K., Harvey, R.P., Moorman, A.F., et al. (2006). Formation of the venous pole of the heart from an Nkx2-5-negative precursor population requires Tbx18. Circ. Res. *98*, 1555–1563.

Cohen, E.D., Wang, Z., Lepore, J.J., Lu, M.M., Taketo, M.M., Epstein, D.J., and Morrisey, E.E. (2007). Wnt/beta-catenin signaling promotes expansion of Isl-1-positive cardiac progenitor cells through regulation of FGF signaling. J. Clin. Invest. *117*, 1794–1804.

Colombo, S., de Sena-Tomás, C., George, V., Werdich, A.A., Kapur, S., MacRae, C.A., and Targoff, K.L. (2018). Nkx genes establish second heart field cardiomyocyte progenitors at the arterial pole and pattern the venous pole through Isl1 repression. Development *145*.

Espinoza-Lewis, R.A., Yu, L., He, F., Liu, H., Tang, R., Shi, J., Sun, X., Martin, J.F., Wang, D., Yang, J., et al. (2009). Shox2 is essential for the differentiation of cardiac pacemaker cells by repressing Nkx2-5. Dev. Biol. *327*, 376–385.

Fukui, H., Miyazaki, T., Chow, R.W., Ishikawa, H., Nakajima, H., Vermot, J., and Mochizuki, N. (2018). Hippo signaling determines the number of venous pole cells that originate from the anterior lateral plate mesoderm in zebrafish. Elife *7*.

George, V., Colombo, S., and Targoff, K.L. (2015). An early requirement for nkx2.5 ensures the first and second heart field ventricular identity and cardiac function into adulthood. Dev. Biol. *400*, 10–22.

Gross-Thebing, T., Paksa, A., and Raz, E. (2014). Simultaneous high-resolution detection of multiple transcripts combined with localization of proteins in whole-mount embryos. BMC Biol. *12*, 55.

Guner-Ataman, B., Paffett-Lugassy, N., Adams, M.S., Nevis, K.R., Jahangiri, L., Obregon, P., Kikuchi, K., Poss, K.D., Burns, C.E., and Burns, C.G. (2013). Zebrafish second heart field development relies on progenitor specification in anterior lateral plate mesoderm and nkx2.5 function. Development *140*, 1353–1363.

Hammerschmidt, M., Pelegri, F., Mullins, M.C., Kane, D.A., Brand, M., van Eeden, F.J., Furutani-Seiki, M., Granato, M., Haffter, P., Heisenberg, C.P., et al. (1996). Mutations affecting morphogenesis during gastrulation and tail formation in the zebrafish, Danio rerio. Development *123*, 143–151.

Han, P., Bloomekatz, J., Ren, J., Zhang, R., Grinstein, J.D., Zhao, L., Burns, C.G., Burns, C.E., Anderson, R.M., and Chi, N.C. (2016). Coordinating cardiomyocyte interactions to direct ventricular chamber morphogenesis. Nature *534*, 700–704.

Hoogaars, W.M., Engel, A., Brons, J.F., Verkerk, A.O., de Lange, F.J., Wong, L.Y., Bakker, M.L., Clout, D.E., Wakker, V., Barnett, P., et al. (2007). Tbx3 controls the sinoatrial node gene program and imposes pacemaker function on the atria. Genes Dev. *21*, 1098–1112.

Huang, C.J., Tu, C.T., Hsiao, C.D., Hsieh, F.J., and Tsai, H.J. (2003). Germ-line transmission of a myocardium-specific GFP transgene reveals critical regulatory elements in the cardiac myosin light chain 2 promoter of zebrafish. Dev. Dyn. *228*, 30–40.

Hurlstone, A.F., Haramis, A.P., Wienholds, E., Begthel, H., Korving, J., Van Eeden, F., Cuppen, E., Zivkovic, D., Plasterk, R.H., and Clevers, H. (2003). The Wnt/beta-catenin pathway regulates cardiac valve formation. Nature *425*, 633–637.

Iyer, D., Gambardella, L., Bernard, W.G., Serrano, F., Mascetti, V.L., Pedersen, R.A., Talasila, A., and Sinha, S. (2015). Robust derivation of epicardium and its differentiated smooth muscle cell progeny from human pluripotent stem cells. Development *142*, 1528–1541.

Jaspard, B., Couffinhal, T., Dufourcq, P., Moreau, C., and Duplàa, C. (2000). Expression pattern of mouse sFRP-1 and mWnt-8 gene during heart morphogenesis. Mech. Dev. *90*, 263–267.

Kapoor, N., Liang, W., Marbán, E., and Cho, H.C. (2013). Direct conversion of quiescent cardiomyocytes to pacemaker cells by expression of Tbx18. Nat. Biotechnol. *31*, 54–62.

Keith, A., and Flack, M. (1907). The form and nature of the muscular connections between the primary divisions of the vertebrate heart. J. Anat. Physiol. *41*, 172–189.

Kilian, B., Mansukoski, H., Barbosa, F.C., Ulrich, F., Tada, M., and Heisenberg, C.P. (2003). The role of Ppt/Wnt5 in regulating cell shape and movement during zebrafish gastrulation. Mech. Dev. *120*, 467–476.

Kwon, C., Arnold, J., Hsiao, E.C., Taketo, M.M., Conklin, B.R., and Srivastava, D. (2007). Canonical Wnt signaling is a positive regulator of mammalian cardiac progenitors. Proc. Natl. Acad. Sci. USA *104*, 10894–10899.

Kwon, C., Qian, L., Cheng, P., Nigam, V., Arnold, J., and Srivastava, D. (2009). A regulatory pathway involving Notch1/beta-catenin/Isl1 determines cardiac progenitor cell fate. Nat. Cell Biol. *11*, 951–957.

Laflamme, M.A., and Murry, C.E. (2011). Heart regeneration. Nature *473*, 326–335.

Lescroart, F., Mohun, T., Meilhac, S.M., Bennett, M., and Buckingham, M. (2012). Lineage tree for the venous pole of the heart: clonal analysis clarifies controversial genealogy based on genetic tracing. Circ. Res. *111*, 1313–1322.

Lewis, J.L., Bonner, J., Modrell, M., Ragland, J.W., Moon, R.T., Dorsky, R.I., and Raible, D.W. (2004). Reiterated Wnt signaling during zebrafish neural crest development. Development *131*, 1299–1308.

Lian, X., Hsiao, C., Wilson, G., Zhu, K., Hazeltine, L.B., Azarin, S.M., Raval, K.K., Zhang, J., Kamp, T.J., and Palecek, S.P. (2012). Robust cardiomyocyte differentiation from human pluripotent stem cells via temporal modulation of canonical Wnt signaling. Proc. Natl. Acad. Sci. USA *109*, E1848–E1857.

Liang, X., Wang, G., Lin, L., Lowe, J., Zhang, Q., Bu, L., Chen, Y., Chen, J., Sun, Y., and Evans, S.M. (2013). HCN4 dynamically marks the first heart field and conduction system precursors. Circ. Res. *113*, 399–407.

Liang, X., Zhang, Q., Cattaneo, P., Zhuang, S., Gong, X., Spann, N.J., Jiang, C., Cao, X., Zhao, X., Zhang, X., et al. (2015). Transcription factor ISL1 is essential for pacemaker development and function. J. Clin. Invest. *125*, 3256–3268.

Lin, L., Cui, L., Zhou, W., Dufort, D., Zhang, X., Cai, C.L., Bu, L., Yang, L., Martin, J., Kemler, R., et al. (2007). Beta-catenin directly regulates Islet1 expression in cardiovascular progenitors and is required for multiple aspects of cardiogenesis. Proc. Natl. Acad. Sci. USA *104*, 9313–9318.

Lindeman, L.C., Vogt-Kielland, L.T., Aleström, P., and Collas, P. (2009). Fish'n ChIPs: chromatin immunoprecipitation in the zebrafish embryo. Methods Mol. Biol. *567*, 75–86.

Liu, P., Wakamiya, M., Shea, M.J., Albrecht, U., Behringer, R.R., and Bradley, A. (1999). Requirement for Wnt3 in vertebrate axis formation. Nat. Genet. *22*, 361–365.

Ma, X., Qu, X., Zhu, W., Li, Y.S., Yuan, S., Zhang, H., Liu, J., Wang, P., Lai, C.S., Zanella, F., et al. (2016). Deterministically patterned biomimetic human iPSC-derived hepatic model via rapid 3D bioprinting. Proc. Natl. Acad. Sci. USA *113*, 2206–2211.

Mathews, E.S., Mawdsley, D.J., Walker, M., Hines, J.H., Pozzoli, M., and Appel, B. (2014). Mutation of 3-hydroxy-3-methylglutaryl CoA synthase I reveals requirements for isoprenoid and cholesterol synthesis in oligodendrocyte migration arrest, axon wrapping, and myelin gene expression. J. Neurosci. *34*, 3402–3412.

Merks, A.M., Swinarski, M., Meyer, A.M., Müller, N.V., Özcan, I., Donat, S., Burger, A., Gilbert, S., Mosimann, C., Abdelilah-Seyfried, S., et al. (2018). Planar cell polarity signalling coordinates heart tube remodelling through tissue-scale polarisation of actomyosin activity. Nat. Commun. *9*, 2161.

Mommersteeg, M.T., Domínguez, J.N., Wiese, C., Norden, J., de Gier-de Vries, C., Burch, J.B., Kispert, A., Brown, N.A., Moorman, A.F., and Christoffels, V.M. (2010). The sinus venosus progenitors separate and diversify from the first and second heart fields early in development. Cardiovasc. Res. *87*, 92–101.

Mommersteeg, M.T., Hoogaars, W.M., Prall, O.W., de Gier-de Vries, C., Wiese, C., Clout, D.E., Papaioannou, V.E., Brown, N.A., Harvey, R.P., Moorman, A.F., et al. (2007). Molecular pathway for the localized formation of the sinoatrial node. Circ. Res. *100*, 354–362.

Moro, E., Ozhan-Kizil, G., Mongera, A., Beis, D., Wierzbicki, C., Young, R.M., Bournele, D., Domenichini, A., Valdivia, L.E., Lum, L., et al. (2012). In vivo Wnt signaling tracing through a transgenic biosensor fish reveals novel activity domains. Dev. Biol. *366*, 327–340.

Nicenboim, J., Malkinson, G., Lupo, T., Asaf, L., Sela, Y., Mayseless, O., Gibbs-Bar, L., Senderovich, N., Hashimshony, T., Shin, M., et al. (2015). Lymphatic vessels arise from specialized angioblasts within a venous niche. Nature *522*, 56–61.

Pradhan, A., and Olsson, P.E. (2014). Juvenile ovary to testis transition in zebrafish involves inhibition of ptges. Biol. Reprod. *91*, 33.

Protze, S.I., Liu, J., Nussinovitch, U., Ohana, L., Backx, P.H., Gepstein, L., and Keller, G.M. (2017). Sinoatrial node cardiomyocytes derived from human pluripotent cells function as a biological pacemaker. Nat. Biotechnol. *35*, 56–68.

Qyang, Y., Martin-Puig, S., Chiravuri, M., Chen, S., Xu, H., Bu, L., Jiang, X., Lin, L., Granger, A., Moretti, A., et al. (2007). The renewal and differentiation of Isl1+ cardiovascular progenitors are controlled by a Wnt/beta-catenin pathway. Cell Stem Cell *1*, 165–179.

Rauch, G.J., Hammerschmidt, M., Blader, P., Schauerte, H.E., Strähle, U., Ingham, P.W., McMahon, A.P., and Haffter, P. (1997). Wnt5 is required for tail formation in the zebrafish embryo. Cold Spring Harb. Symp. Quant. Biol. *62*, 227–234.

Schumacher, J.A., Bloomekatz, J., Garavito-Aguilar, Z.V., and Yelon, D. (2013). tal1 Regulates the formation of intercellular junctions and the maintenance of identity in the endocardium. Dev. Biol. *383*, 214–226.

Stanley, E.G., Biben, C., Elefanty, A., Barnett, L., Koentgen, F., Robb, L., and Harvey, R.P. (2002). Efficient Cre-mediated deletion in cardiac progenitor cells conferred by a 3′UTR-ires-Cre allele of the homeobox gene Nkx2-5. Int. J. Dev. Biol. *46*, 431–439.

Stieber, J., Herrmann, S., Feil, S., Löster, J., Feil, R., Biel, M., Hofmann, F., and Ludwig, A. (2003). The hyperpolarization-activated channel HCN4 is required for the generation of pacemaker action potentials in the embryonic heart. Proc. Natl. Acad. Sci. USA *100*, 15235–15240.

Stoick-Cooper, C.L., Weidinger, G., Riehle, K.J., Hubbert, C., Major, M.B., Fausto, N., and Moon, R.T. (2007). Distinct Wnt signaling pathways have opposing roles in appendage regeneration. Development *134*, 479–489.

Sun, Y., Liang, X., Najafi, N., Cass, M., Lin, L., Cai, C.L., Chen, J., and Evans, S.M. (2007). Islet 1 is expressed in distinct cardiovascular lineages, including pacemaker and coronary vascular cells. Dev. Biol. *304*, 286–296.

Targoff, K.L., Colombo, S., George, V., Schell, T., Kim, S.H., Solnica-Krezel, L., and Yelon, D. (2013). Nkx genes are essential for maintenance of ventricular identity. Development *140*, 4203–4213.

Tessadori, F., van Weerd, J.H., Burkhard, S.B., Verkerk, A.O., de Pater, E., Boukens, B.J., Vink, A., Christoffels, V.M., and Bakkers, J. (2012). Identification and functional characterization of cardiac pacemaker cells in zebrafish. PLoS One *7*, e47644.

Trautwein, W., and Uchizono, K. (1963). Electron microscopic and electrophysiologic study of the pacemaker in the sino-atrial node of the rabbit heart. Z. Zellforch Microsk Anat. *61*, 96–109.

Ueno, S., Weidinger, G., Osugi, T., Kohn, A.D., Golob, J.L., Pabon, L., Reinecke, H., Moon, R.T., and Murry, C.E. (2007). Biphasic role for Wnt/beta-catenin signaling in cardiac specification in zebrafish and embryonic stem cells. Proc. Natl. Acad. Sci. USA *104*, 9685–9690.

van Weerd, J.H., and Christoffels, V.M. (2016). The formation and function of the cardiac conduction system. Development *143*, 197–210.

Vedantham, V., Galang, G., Evangelista, M., Deo, R.C., and Srivastava, D. (2015). RNA sequencing of mouse sinoatrial node reveals an upstream regulatory role for Islet-1 in cardiac pacemaker cells. Circ. Res. *116*, 797–803.

Veevers, J., Farah, E.N., Corselli, M., Witty, A.D., Palomares, K., Vidal, J.G., Emre, N., Carson, C.T., Ouyang, K., Liu, C., et al. (2018). Cell-surface marker signature for enrichment of ventricular cardiomyocytes derived from human embryonic stem cells. Stem Cell Rep *11*, 828–841.

Wada, R., Muraoka, N., Inagawa, K., Yamakawa, H., Miyamoto, K., Sadahiro, T., Umei, T., Kaneda, R., Suzuki, T., Kamiya, K., et al. (2013). Induction of human cardiomyocyte-like cells from fibroblasts by defined factors. Proc. Natl. Acad. Sci. USA *110*, 12667–12672.

Wang, J., Bai, Y., Li, N., Ye, W., Zhang, M., Greene, S.B., Tao, Y., Chen, Y., Wehrens, X.H., and Martin, J.F. (2014). Pitx2-microRNA pathway that delimits sinoatrial node development and inhibits predisposition to atrial fibrillation. Proc. Natl. Acad. Sci. USA *111*, 9181–9186.

Wiese, C., Grieskamp, T., Airik, R., Mommersteeg, M.T., Gardiwal, A., de Gier-de Vries, C., Schuster-Gossler, K., Moorman, A.F., Kispert, A., and Christoffels, V.M. (2009). Formation of the sinus node head and differentiation of sinus node myocardium are independently regulated by Tbx18 and Tbx3. Circ. Res. *104*, 388–397.

Witty, A.D., Mihic, A., Tam, R.Y., Fisher, S.A., Mikryukov, A., Shoichet, M.S., Li, R.K., Kattman, S.J., and Keller, G. (2014). Generation of the epicardial lineage from human pluripotent stem cells. Nat. Biotechnol. *32*, 1026–1035.

Yelon, D., Horne, S.A., and Stainier, D.Y. (1999). Restricted expression of cardiac myosin genes reveals regulated aspects of heart tube assembly in zebrafish. Dev. Biol. *214*, 23–37.

Zhang, R., Han, P., Yang, H., Ouyang, K., Lee, D., Lin, Y.F., Ocorr, K., Kang, G., Chen, J., Stainier, D.Y., et al. (2013). In vivo cardiac reprogramming contributes to zebrafish heart regeneration. Nature *498*, 497–501.

Zhou, Y., Cashman, T.J., Nevis, K.R., Obregon, P., Carney, S.A., Liu, Y., Gu, A., Mosimann, C., Sondalle, S., Peterson, R.E., et al. (2011). Latent TGF-beta binding protein 3 identifies a second heart field in zebrafish. Nature *474*, 645–648.

STAR★METHODS

KEY RESOURCES TABLE

REAGENT or RESOURCE	SOURCE	IDENTIFIER
Antibodies		
Rabbit anti-dsRed antibody	Clontech	Cat# 632496
Rabbit anti-Isl1 antibody	Genetex	Cat# GTX128201
Mouse anti-Isl1 antibody	DSHB	Cat# 39.4D5; RRID: AB_2314683
Mouse anti-MF20 antibody	DSHB	Cat# MF20; RRID: AB_2147781
Rabbit anti-Nkx2.5 anitibody	Genetex	Cat# GTX128357
Rabbit anti-phospho-histone H3 antibody	Upstate	Cat# 06-570; RRID: AB_310177
Anti-Digoxigenin-AP, Fab fragments	Sigma Aldrich	Cat# 11093274910; RRID: AB_2734716
Mouse anti β-catenin antibody	BD Biosciences	Cat# 610153; RRID: AB_397554
Mouse IgG antibody	Invitrogen	Cat# 02-6502
Chicken anti-GFP antibody	Aves Labs	Cat# GFP-1020; RRID: AB_10000240
Rabbit anti-human NKX2-5 antibody	Cell signaling	Cat# 8792; RRID: AB_2797667
Mouse anti-human SHOX2 antibody	Abcam	Cat# ab55740; RRID: AB_945451
Goat anti-rabbit IgG-Alexa 568	Thermo Fisher Scientific	Cat# A-11011; RRID: AB_143157
Goat anti-mouse IgG Cy5	Thermo Fisher Scientific	Cat# A-10524; RRID: AB_2534033
Goat anti-mouse IgG-Alexa 405	Thermo Fisher Scientific	Cat# A-31553; RRID: AB_221604
Goat anti-rabbit IgG-Alexa 488	Thermo Fisher Scientific	Cat# A-11008; RRID: AB_143165
Goat anti-chicken IgG-Alexa 488	Thermo Fisher Scientific	Cat# A-11039; RRID: AB_2534096
Goat anti-rabbit IgG Cy5	Thermo Fisher Scientific	Cat# A-10523; RRID: AB_2534032
Goat anti-mouse IgG-Alexa 568	Thermo Fisher Scientific	Cat# A-11004; RRID: AB_2534072
Chemicals, Peptides, and Recombinant Proteins		
PNU-74654	Sigma Aldrich	Cat# P0052
CHIR99021	Sigma Aldrich	Cat# SML1046
CHIR99021	Tocris	Cat# 4423
TNP-470	Sigma Aldrich	Cat# T1455
IWP2	Tocris	Cat# 3533
2,3-butanedione monoxime	Sigma Aldrich	Cat# B0753
Human Wnt5b protein	R&D systems	Cat# 7347-WN
Critical Commercial Assays		
in situ cell death detection kit, TMR red	Roche	Cat# 12156792910
RNAscope Multiplex Fluorescent Reagent Kit v2	ACD Bio	Cat# 323100
RNAscope *Dr-wnt5b Probe C1*	ACD Bio	Cat# 579321-C1
RNeasy mini kit	Qiagen	Cat# 74104
Superscript III kit	Invitrogen	Cat# 18080051
Power SYBR Green Master Mix	Thermo Fisher Scientific	Cat# 4367659
Experimental Models: Cell Lines		
Human: H9-hTnnTZ-pGZ-D2 human embryonic stem cells	WiCell	H9-hTnnTZ-pGZ-D2
Experimental Models: Organisms/Strains		
Zebrafish: *TgBAC(-36nkx2.5:Kaede)*	Burns Lab, Massachusetts General Hospital	fb9Tg
Zebrafish: *Tg(myl7:Cerulean)*	Appel Lab, University of Colorado Denver	co19Tg
Zebrafish: *Tg(hsp70l:nkx2.5-EGFP)*	Targoff Lab, Columbia University	fcu1Tg
Zebrafish: *Tg(7xTCF-Xla.Siam:nlsmCherry)*	Argenton Lab, University of Padova	ia5Tg
Zebrafish: *Tg(-36nkx2.5:ZsYellow)*	Burns Lab, Massachusetts General Hospital	fb7Tg

(*Continued on next page*)

Continued		
REAGENT or RESOURCE	SOURCE	IDENTIFIER
Zebrafish: *Tg(myl7:eGFP)*	Tsai Lab, National Taiwan University	twu277Tg
Zebrafish: *Tg(hsp70:dnTCF-GFP)*	David Raible Lab, University of Washington	w26Tg
Zebrafish: *Tg(myl7:gCaMP)*	Stainier Lab, Max Planck Institute for Heart and Lung Research	s878Tg
Zebrafish: *Tg(hsp70l:wnt5b-GFP)*	Randall Moon Lab, University of Washington	w33Tg
Zebrafish: *Tg(myl7:H2A-mCherry)*	Yelon Lab, University of California, San Diego	sd12Tg
Zebrafish: *Tg(amhc:eGFP)*	Stainier Lab, Max Planck Institute for Heart and Lung Research	s958Tg
Zebrafish: *nkx2.5$^{vu179/vu179}$*	Lila Solnica-Krezel Lab, Vanderbilt University	vu179
Zebrafish: *wnt5b $^{ta98/ta98}$*	Nusslein-Volhard Lab, Planck Institute for Heart and Lung Research	ta98
Zebrafish: *apc$^{sd58/sd58}$*	this manuscript	sd58
Oligonucleotides		
Primers for ChIP-qPCR, see Table S2	this paper	N/A
Primers for qRT-PCR, see Table S3	this paper	N/A
Software and Algorithms		
Nikon NIS Elements software	Nikon	N/A
Fiji/ImageJ	NIH	https://imagej.net/Fiji/Downloads
Adobe Photoshop CS5	Adobe	N/A
FlowJo version 10	FlowJo	https://www.flowjo.com/solutions/flowjo/downloads
GraphPad Prism 7	GraphPad	N/A
pClamp 10.3 software	Molecular Devices	N/A

LEAD CONTACT AND MATERIALS AVAILABILITY

Further information and requests for resources and reagents should be directed to and will be fulfilled by the Lead Contact, Neil C. Chi (nchi@ucsd.edu). The *apc^{sd58}* mutant zebrafish generated in this study is available upon request.

EXPERIMENTAL MODEL AND SUBJECT DETAILS

Animals

Zebrafish (*Danio rerio*) were raised under standard laboratory conditions at 28°C on a 14 hours light /10 hours dark cycle. All the embryos used in this study were collected by natural spawning and incubated in egg water in a 28°C incubator. All animal work was approved by the University of California at San Diego Institutional Animal Care and Use Committee (IACUC). The following established transgenic and mutant lines were used: *TgBAC(-36nkx2.5:Kaede)^{fb9}* (Guner-Ataman et al., 2013) abbreviated as *Tg(nkx2.5:Kaede)*; *Tg(myl7:Cerulean)^{co19}*(Mathews et al., 2014); *Tg(hsp70l:nkx2.5-EGFP)^{fcu1}*(George et al., 2015) abbreviated as *Tg(hsp70:nkx2.5)*; *Tg(7xTCF-Xla.Siam:nlsmCherry)^{ia5}*(Moro et al., 2012) abbreviated as *Tg(TCF:nlsmCherry)*; *Tg(-36nkx2.5:ZsYellow)^{fb7}*(Zhou et al., 2011) abbreviated as *Tg(nkx2.5:ZsYellow)*; *Tg(myl7:eGFP)^{twu277}*(Huang et al., 2003); *Tg(hsp70:dnTCF-GFP)^{w26}*(Lewis et al., 2004) abbreviated as *Tg(hsp70:dnTCF)*; *Tg(myl7:gCaMP)^{s878}*(Chi et al., 2008); *Tg(hsp70l:wnt5b-GFP)^{w33}*(Stoick-Cooper et al., 2007) abbreviated as *Tg(hsp70:wnt5b)*; *Tg(myl7:H2A-mCherry)^{sd12}*(Schumacher et al., 2013); *Tg(amhc:eGFP)^{s958}*(Zhang et al., 2013); *nkx2.5^{vu179}*(Targoff et al., 2013) and *wnt5b ^{ta98}* designated as *pipetail* (*ppt*) (Hammerschmidt et al., 1996; Rauch et al., 1997). Homozygous *nkx2.5^{vu179}* or *ppt* mutant embryos were identified using previously characterized defects in cardiac chamber morphology (Targoff et al., 2013) or body axis elongation (Hammerschmidt et al., 1996; Rauch et al., 1997), respectively. The zebrafish embryos used for experiments were less than 48 hpf, a stage at which sex can not be readily determined.

The *apc^{sd58}* allele was discovered in a previous forward genetic screen performed at UCSD. Microsatellite markers and bulk segregant analysis were used to map the *sd58* allele to chromosome 10. Additional fine genetic mapping using individual homozygous mutant embryos placed the *sd58* allele near the microsatellite marker z7316 and the *apc* gene. Sequencing of the *apc* gene in *sd58* homozygous mutant embryos uncovered a nonsense mutation at amino acid position 1018 (Figure 4A). Furthermore, we found that an independent loss-of-function *apc* allele, *apc^{hu745}* (Hurlstone et al., 2003), failed to complement the *sd58* allele (data not shown). Increased *TCF*:nlsmCherry expression confirmed constitutive activation of canonical Wnt signaling in *apc^{sd58}* mutants (Figures 4D–4E′).

Human Pluripotent Stem Cells

H9-hTnnTZ-pGZ-D2 human embryonic stem cell line was purchased from WiCell and maintained on Geltrex (Gibco) coated plates in E8 medium. They are female cells and have been authenticated by Short Tandem Repeat (STR) profiling analysis.

METHOD DETAILS

Nkx2.5 Photoconversion Studies

Tg(nkx2.5:Kaede) embryos were first mounted in 1% low melting point agarose (Lonza) in 35-mm glass bottom petri dishes (MatTek). A selected region of interest was then exposed to UV light for 1 min using a 405-nm blue diode laser on a Leica SP5 confocal laser scanning microscope, with a HCX IRAPO L 25.0X/0.95 water immersion objective. Following photoconversion and imaging, embryos were removed from the agarose, raised in the dark until 24 hpf, confirmed to display wild-type morphology and then fixed for immunofluorescence studies as described below.

Heat Shock Induction and Small Molecule Inhibitor Studies in Zebrafish

Heat-shock induction was conducted as previously described (Han et al., 2016). Briefly, embryos containing heat-shock transgenes or wild-type siblings at specified stages were placed into a 37°C incubator for 30 minutes, followed by 3 minutes in a 42°C water bath. Embryos were then returned to a 28°C incubator prior to their subsequent analysis.

For small molecule inhibitor studies, zebrafish embryos were incubated in either 0.1% DMSO (control) or respective small molecule inhibitor between 16 ss and 24 hpf. Specific inhibitors and the concentration used are detailed in Table S1.

In Situ Hybridization, Immunofluorescence, TUNEL Assays in Zebrafish

Whole mount *in situ* hybridization and immunofluorescence were performed as previously described (Zhang et al., 2013). The *in situ* probes and primary antibodies used in this study include: *hcn4* (ZDB-GENE-050420-360), *isl1* (ZDB-GENE-980526-112), *shox2* (ZDB-GENE-040426-1457), *tbx18* (ZDB-GENE-020529-2), *wnt5b* (ZDB-GENE-980526-87), anti-dsRed (rabbit, Clontech,1:2000), anti-Isl1 (rabbit, GeneTex, 1:1000), anti-Isl1 (mouse, Developmental Studies Hybridoma Bank, 1:100), anti-MF20 (mouse, Developmental Studies Hybridoma Bank, 1:100), anti-Nkx2.5 (rabbit, GeneTex, 1:50), and anti-phospho-histone H3 (rabbit, Upstate, 1:200). *in situ* probes were detected with Anti-Digoxigenin-AP antibody (Fab fragments, Roche) for *in situ* hybridization, while primary antibodies were detected with the following appropriate secondary antibodies for immunofluorescence: anti-rabbit IgG-Alexa 568 (goat, Life technologies, 1:250), anti-mouse IgG Cy5 (goat, Life technologies, 1:250), anti-mouse IgG-Alexa 405 (goat, Life technologies, 1:250) and anti-rabbit IgG-Alexa 488 (goat, Life technologies, 1:250).

Cell death was detected using the *in situ* cell death detection kit (TMR red, Roche). Zebrafish embryos were fixed with 4% paraformaldehyde (PFA) for 2 hours, permeabilized with 0.5% TritonX-100 in PBS and incubated in TUNEL staining solution at 37°C for 2 hours. Fluorescent images were obtained using a Nikon C2 confocal microscope.

RNAscope *In Situ* Hybridization

Zebrafish whole mount staining using the RNAscope Multiplex Fluorescent Reagent Kit v2 (ACD Bio) was performed as described previously (Gross-Thebing et al., 2014) with modifications. Briefly, 17 hpf embryos were fixed for 1 hour in 4% paraformaldehyde, washed with PBST (PBS with 0.1%Tween), and dehydrated in MeOH at −20°C overnight. Embryos were dried for 30 minutes at room temperature before Protease III treatment. RNAscope *Dr-wnt5b Probe C1* (ACD Bio) was hybridized overnight at 40°C. Embryos were postfixed with 4% paraformaldehyde and washed with 0.2× SSCT before the amplification steps (Amp1-3). To develop the probe signal, embryos were treated with HRP-C1 before Opal 570 dye (Akoya Biosciences, diluted in TSA buffer) incubation, and then treated with HRP-blocker. Fluorescent images were obtained using a Nikon C2 confocal microscope.

Optical Mapping for Zebrafish Embryos

Optical mapping was performed as previously described (Chi et al., 2008). Briefly, individual *Tg(myl7:gCaMP)* zebrafish embryos at 48 hpf were treated with 10 mM 2,3-butanedione monoxime (Sigma) for 15 minutes to achieve electro-mechanical uncoupling. Embryos were then mounted in 1% low melting point agarose (Lonza) in 35 mm glass bottom petri dishes (MatTek). Epifluorescence images of the heart were obtained with a Nikon Eclipse Ti inverted microscope, using a 20× Plan Apo air objective, a Nikon INTENSILIGHT C-HGFIE Precentered Fiber Illuminator, and standard fluorescein isothiocyanate filter set. Real-time images were captured with an Andor iXon EMCCD camera at a frame rate of 60 ms/frame and processed as described in the Quantification and Statistical Analysis section.

Chromatin Immunoprecipitation (ChIP) Studies

Using the GRC Zv9 zebrafish genome assembly, regulatory regions of *isl1* or *tbx18* genes were interrogated to discover putative TCF/LEF binding sites based on the TCF/LEF consensus sequences CAAAGG (Lin et al., 2007). Identified sites were then matched to previously published regions of H3K27ac and H3K4me1 occupancy (i.e. active enhancers) in the genome of 24 hpf zebrafish embryos (GEO: GSE32483) (Bogdanovic et al., 2012). Primers (see Table S2) were then designed to span these overlapping regions for

ChIP quantitative PCR (qPCR) studies. An illustration designating the location of the putative TCF/LEF binding sites (Site 1) and possible active enhancer peaks can be found in Figures S5A–S5D. Negative control primers were located in non-coding regions (Site 2) at least 1.5 kb away from the putative TCF/LEF sites.

ChIP was performed as previously described (Lindeman et al., 2009) with modifications. Briefly, ~800 wild-type embryos at 21-23 ss were collected, homogenized and cross-linked by incubation in 1% formaldehyde. The chromatin was sonicated to generate ~500 base-pair fragments and pre-cleared with protein A agarose beads (Upstate). Equal amounts of soluble chromatin were incubated with anti-β-catenin antibody (mouse, BD Biosciences), which has been previously used for ChIP (Cha et al., 2016), or control IgG antibody (mouse, Invitrogen). After overnight antibody incubations, protein A agarose beads were added to collect the antibody-chromatin complex. Chromatin fragments were then eluted, reverse cross-linked and purified. These DNA fragments were then used for qPCR in combination with primers spanning the putative TCF/LEF (and control) sites as described above. qPCR was performed on a CFX Connect Real-Time PCR Detection System (Bio-Rad) using Power SYBR Green Master Mix (Thermo Fisher Scientific). Values were normalized using the percent input method.

Human Pluripotent Stem Cell (hPSC) Studies

Differentiation of hPSCs into cardiomyocytes was performed using established protocols as previously described (Lian et al., 2012). Briefly, H9-hTnnTZ-pGZ-D2 (WiCell) human embryonic stem cells (hESCs) were expanded to 80% confluency on Geltrex (Gibco) coated plates in E8 medium. On D0, cells were cultured with RPMI/B27 without insulin (culture media) containing 12 μM CHIR. After 24 hours, CHIR-treated media was removed and cells were cultured for 48 hours in culture media only. On D3, 5 μM IWP2 was then added to culture media. On D5, this culture media was then replaced with culture media containing 3 μM CHIR or 1000 ng/ml WNT5B (R&D systems) to induce pacemaker cardiomyocyte differentiation, or DMSO or HSA (human serum albumin) to induce control cardiomyocyte differentiation. On D7 and onwards, cells were then maintained in culture media + insulin only. Small molecule inhibitors used for the differentiation are detailed in Table S1. Using a BD Influx cell sorter (BD Biosciences), differentiating D15 hPSCs were sorted based on *TNNT2:*GFP expression and side-scatter to collect *TNNT2:*GFP+ cardiomyocytes and *TNNT2:*GFP- non-cardiomyocytes.

For real-time quantitative reverse transcriptase (qRT)-PCR analysis, RNA was extracted from cells (RNeasy mini kit, Qiagen) and used to produce cDNA (Superscript III kit, Invitrogen). qRT-PCR was performed on a CFX Connect Real-Time PCR Detection System (Bio-Rad) using Power SYBR Green Master Mix (Thermo Fisher Scientific). RNA expression levels were based on averaging qRT-PCR results measured from three independent cardiomyocyte differentiations. The housekeeping TATA box binding protein (*TBP*) gene was used to normalize RNA expression levels. Primer sequences are listed in Table S3.

For immunofluorescence staining, sorted D15 *TNNT2:*GFP+ cells were replated, cultured for another four days and then fixed. Immunofluorescence staining was performed as previously described (Witty et al., 2014) using the following primary antibodies: anti-GFP (chicken, Aves Labs, 1:200), anti-human NKX2-5 (rabbit, cell signaling,1:800) and anti-human SHOX2 (mouse, Abcam, 1:200). The following secondary antibodies were used: anti-chicken IgG-Alexa 488 (goat, Life technologies, 1:400), anti-rabbit IgG Cy5 (goat, Life technologies, 1:400), and anti-mouse IgG-Alexa 568 (goat, Life technologies, 1:400). DAPI (1 μg/ml, Roche) staining was used to identify nuclei. Stained cells were visualized using a Nikon C2 confocal microscope.

Electrophysiology

Action potentials were recorded as previously described (Veevers et al., 2018). Specifically, *TNNT2:*GFP+ cells were sorted, replated on plastic bottom dishes and cultured for an additional 4 days as described in the hPSC studies section. Single cell spontaneous action potentials were recorded under whole-cell current-clamp conditions with a patch pipette resistance of 3-5 MΩ. Cells were incubated in an external solution containing: 150 mM NaCl, 5 mM KCl, 1 mM $CaCl_2$, 1 mM $MgCl_2$, 10 mM HEPES and 10 mM glucose (adjusted to pH 7.4, with NaOH). The intracellular pipette solution used for cell electrophysiology studies contained the following: 150 mM KCl, 5 mM NaCl, 1 mM $MgCl_2$, 2 mM EGTA, 1 mM MgATP, 10 mM HEPES (adjusted to pH 7.2 with KOH). Patch clamp recordings were performed using an Axopatch 200B amplifier and pClamp 10.3 software (Molecular devices, LLC). All experiments were performed at room temperature (20–22°C).

3D Bioprinting and Optical Mapping of hPSC-Derived Cardiomyocyte "Mini Hearts"

To bioprint hPSC-derived cardiomyocyte mini hearts, *TNNT2:*GFP hPSCs were initially differentiated into D15 cardiomyocytes as described in the hPSC studies section. These hPSC-cardiomyocytes were then FACS sorted based on *TNNT2:*GFP expression and resuspended at 200 million cardiomyocytes/ml. This hPSC-cardiomyocyte suspension was mixed at a 1:1 ratio with a pre-warmed prepolymer solution consisting of 10% (wt/vol) gelatin methacrylate (GelMA), which was synthesized as previously reported (Ma et al., 2016), and 0.3% (wt/vol) lithium phenyl-2 4 6-trimethylbenzoylphosphinate (LAP) (Ma et al., 2016). The two-step process to bioprint a 3D heart-shaped construct involves printing D15 hPSC-cardiomyocytes that were treated with DMSO from D5-7 into a heart-shape with a circular region missing in the upper left region, followed by printing a complementary circular structure containing D15 hPSC-cardiomyocytes that were either treated with CHIR or DMSO (control) from D5-7 into the empty region. For each printing step, 20 μl of cell-material mixture was pipetted into the space between a methacrylated coverslip fixed on the motion controller stage and a polydimethylsiloxane (PDMS) film attached to a glass slide. UV light (88 mW/cm^2) was projected to the stage after loading the first pattern into a digital micromirror device (DMD) chip. This first bioprinted structure was washed three times with warm PBS and aspirated dry. The second cell-material mixture was then pipetted into the space between the same coverslip and PDMS film for

a second light exposure. Afterwards, the bioprinted sample was washed in both PBS and media, and then incubated at 37°C with 5% CO_2. Culture media was replaced every other day. The height of the construct was set to be 200 μm to allow sufficient oxygen diffusion within the hydrogel encapsulating the cardiomyocytes.

Optical mapping for the 3D bioprinted hearts was performed 7 days after printing. Coverslips with 3D bioprinted mini hearts were placed into 35-mm glass bottom petri dishes (MatTek). Mini heart cardiomyocytes were loaded with 10 μM Rhod2-AM (Molecular Probes) for 20 min at 37°C, and then epifluorescence images were obtained with a Nikon Eclipse Ti inverted microscope, using 10× Plan Apo air objective, a Nikon INTENSILIGHT C-HGFIE Precentered Fiber Illuminator, and standard tetramethylrhodamine filter set. Real-time images were acquired with an Andor iXon EMCCD camera at a frame rate of 40 ms/frame and processed as described in the Quantification and Statistical Analysis section.

Cardiomyocyte Beating Rate Analysis

To examine cardiomyocyte beating rate, *TNNT2:*GFP+ cells were sorted as described in the hPSC studies section, replated at low density and cultured for another 4 days before the beating rate of individual cardiomyocytes was manually counted. For 3D mini heart beating rate analysis, the beating rate for each mini heart was manually counted 7 days after printing when mini heart beating is synchronized.

QUANTIFICATION AND STATISTICAL ANALYSIS

All fluorescent images were obtained with a Nikon C2 confocal microscope or a Nikon Eclipse Ti inverted fluorescence microscope coupled with an Andor iXon EMCCD camera, and processed using Nikon NIS Elements software, ImageJ and Adobe Photoshop. To count cell numbers, 3D-reconstructions from individual confocal slices were used for manual quantification. To determine the average percentage of Shox2+ or Nkx2.5- hPSC-cardiomyocytes derived from hPSC-cardiac progenitors treated with DMSO or CHIR between D5-7, eight and nine equally-sized microscope images (210 sq microns) were respectively examined from representative regions across three independent cardiomyocyte differentiations for DMSO and CHIR conditions. As a result, a total of 812 and 729 hPSC-cardiomyocytes were analyzed for DMSO or CHIR treatment conditions, respectively. To determine the average percentage of Shox2+ or Nkx2.5- hPSC-cardiomyocytes derived from hPSC-cardiac progenitors treated with HSA or WNT5B between D5-7, eight equally-sized microscope images (210 sq microns) were respectively examined from representative regions across three independent cardiomyocyte differentiations for HSA and WNT5B conditions. As a result, a total of 756 and 612 hPSC-cardiomyocytes were analyzed for HSA or WNT5B treatment conditions, respectively. For optical mapping of calcium activation, images were processed by first identifying the minimum and the maximum values of each pixel across all time points. These values were used to normalize the recorded fluorescence signal intensity at individual time points. Isochronal lines at 60 or 40 ms intervals were drawn as contiguous lines across the maximal fluorescent pixels (Chi et al., 2008). No statistical methods were used to predetermine sample size. Animals were assigned to experimental groups using simple randomization, without investigator blinding. Unpaired two-tailed Student's t-tests were used to determine statistical significance. $p < 0.05$ was considered to be statistically significant, as indicated by an asterisk. The standard error of the mean (s.e.m.) was used for error bars.

DATA AND CODE AVAILABILITY

This study did not generate any datasets or code.